International Immunopharmacology 170 (2026) 116038

Contents lists available at ScienceDirect

International Immunopharmacology

journal homepage: www.elsevier.com/locate/intimp

S-methylmethionine ameliorates renal injury in diabetic mice by modulating macrophage inflammaging *via* ERK/NF-κb signaling pathway

Hao Dong [a,b], Linjie Shen [a,b], Pawuziya Abulizi [a,c], Yuezhang Sun [a,b], Lulingxiao Nie [a], Aimin Cui [a,b], Qian Fu [a,b], Ning Ji [a], Yuwen Luo [a], Chienshan Chen [d], Aimin Xu [e], Wai Keung Leung [f,*], Qi Wang [a,b,**]

[a] *State Key Laboratory of Oral Diseases & National Center for Stomatology & National Clinical Research Center for Oral Diseases, West China Hospital of Stomatology, Sichuan University, Chengdu, China.*
[b] *Department of Prosthodontics, West China Hospital of Stomatology, Sichuan University, Chengdu, China.*
[c] *Department of Prosthodontics, Longgang E.N.T Hospital & Shenzhen Key Laboratory of E.N.T, Institute of E.N.T Shenzhen, Shenzhen, China.*
[d] *College of Chinese Medicine, Chengdu University of Traditional Chinese Medicine, Chengdu, China.*
[e] *State Key Laboratory of Pharmaceutical Biotechnology & Department of Pharmacology and Pharmacy & Department of Medicine, the University of Hong Kong, Hong Kong, SAR, China.*
[f] *Faculty of Dentistry, the University of Hong Kong, Prince Philip Dental Hospital, 34 Hospital Road, Sai Ying Pun, Hong Kong SAR, China.*

A R T I C L E I N F O

Editor Name: Dr. Thomas Petro

Keywords:
Diabetic kidney disease
S-methylmethionine
Macrophage
Inflammaging
ERK
NF-κB

A B S T R A C T

Diabetic kidney disease (DKD) is a major microvascular complication of diabetes, yet current therapeutic strategies remain insufficient to halt its progression. Emerging evidence suggests that macrophage-mediated inflammaging is a key pathogenic mechanism underlying diabetic renal injury, but effective targeted interventions are still limited. In this study, we identify *S*-Methylmethionine (SMM) as a candidate therapeutic compound capable of modulating macrophage inflammaging, and systematically evaluate its protective potential. In streptozotocin-induced diabetic mice, SMM markedly improved renal function in a dose-dependent manner, alleviating glomerular hypertrophy, mesangial expansion, and fibrosis, accompanied by reductions in biomarkers of kidney injury. The transcriptomic analysis of kidney tissues from patients with DKD revealed enrichment of aging- and inflammation-related pathways, which were effectively suppressed by SMM. SMM attenuated macrophage inflammaging by inhibiting proinflammatory cytokines release, reducing the expression of senescence-associated proteins, and promoting a shift in macrophage polarization toward a reparative phenotype. SMM also blocked phosphorylation and nuclear translocation of ERK and NF-κB p65, thereby repressing downstream inflammatory and senescence gene expression programs. Collectively, these findings establish SMM as a novel modulator of macrophage inflammaging and highlight its therapeutic potential for the treatment of DKD.

1. Introduction

Diabetic kidney disease (DKD) is one of the most common microvascular complications of diabetes, and remains the leading cause of chronic kidney disease (CKD) and end-stage renal disease (ESRD) worldwide [1–3]. The pathological mechanisms of DKD are complex, involving intricate interactions among hyperglycemia, oxidative stress, and hemodynamic dysfunction [4,5]. However, current intervention strategies targeting glycemic control and renin-angiotensin system blockade fail to effectively prevent DKD progression [6]. The action to control cardiovascular risk in diabetes-memory in diabetes (ACCORD-MIND) trial reported that intensive glycemic control appears to have no effect on development of ESRD [7]. Therefore, identifying new therapeutic targets and agents holds significant importance for the effective prevention and treatment of DKD.

Inflammaging refers to the chronic low-grade inflammation present in aging or age-related diseases, characterized by a self-perpetuating cycle between chronic inflammation and senescence [8].

* Corresponding author at: Faculty of Dentistry, the University of Hong Kong, Prince Philip Dental Hospital, 34 Hospital Road, Sai Ying Pun, Hong Kong SAR, China.
** Corresponding author at: West China Hospital of Stomatology, Sichuan University, 14 3rd Section S Renmin Road, Chengdu, China, 610041.
E-mail addresses: ewkleung@hku.hk (W.K. Leung), wqinno8751@gmail.com (Q. Wang).

https://doi.org/10.1016/j.intimp.2025.116038
Received 23 October 2025; Received in revised form 29 November 2025; Accepted 10 December 2025
Available online 20 December 2025

Accumulating evidence has revealed the critical role of inflammaging in diabetes-related dysfunction and the progression of diabetic complications [9–11]. Metabolic disorders such as hyperglycemia induce a chronic low-grade inflammatory state in the body, leading to cellular senescence or premature aging [12]. Senescent cells release a series of pro-inflammatory mediators known as the senescence-associated secretory phenotype (SASP), further amplifying inflammatory responses and tissue damage [13]. Macrophages are central contributors to inflammaging and represent one of the primary sources of SASP [14]. Macrophages display remarkable plasticity and can adopt proinflammatory or reparative phenotypes in response to distinct environmental cues [15]. In diabetes, macrophage populations shift toward a proinflammatory state that increases cytokine production, matrix degradation, and cellular stress [16]. At the same time, macrophages exposed to chronic metabolic stress may develop senescence-related features that impair phagocytosis, migration, and tissue repair [17,18]. Recent studies have shown that modulating inflammation and senescence in macrophages can help prevent and manage diabetic complications such as retinopathy [19,20]. Restoring macrophage homeostasis and preventing macrophage inflammaging therefore represents a promising approach to protect renal structure and function in DKD.

Numerous studies have demonstrated that the extracellular signal-regulated kinase (ERK) / nuclear factor kappa B (NF-κB) pathway plays a pivotal role in regulating inflammaging in DKD [21–23]. As a key member of the mitogen-activated protein kinase (MAPK) family, ERK participates in integrating multiple critical pathways governing metabolism and inflammation [24]. High glucose mediates the phosphorylation and activation of ERK signaling pathways, and the level of phosphorylated ERK is closely associated with the progression of multiple diabetic complications [25]. NF-κB, as a major regulator of inflammatory and aging gene networks, enhances the release of SASP and exacerbates tissue damage [26]. The ERK signaling pathway regulates NF-κB activity through phosphorylation cascades. Under high glucose conditions, activated ERK directly phosphorylates NF-κB subunits, promoting their nuclear translocation and enhancing the transcription of downstream target genes. In addition, NF-κB-driven SASP further amplifies ERK signaling, establishing a self-reinforcing loop. The sustained activation of the ERK/NF-κB pathway contributes to inflammaging, which may represent a key mechanism underlying the progression of diabetic kidney injury. These findings suggest that modulating inflammaging through targeting the ERK/NF-κB axis could offer a potential strategy for delaying DKD progression.

Recent studies have revealed the potential role of *S*-methylmethionine (SMM, also referred to as Vitamin U) in alleviating inflammatory responses and reducing senescence [27,28]. SMM is a naturally-derived amino acid widely present in vegetables such as cabbage, kale, and garlic [29]. Pharmacological studies have revealed its multiple bioactivities, including anti-ulcer, antioxidant stress, and metabolic regulatory functions, demonstrating promising therapeutic effects against liver toxicity and brain injury induced by various toxic compounds [27,30]. However, the role of SMM in DKD and its potential regulatory mechanisms for macrophage inflammaging remain unexplored.

In this study, we evaluated the pharmacological effects of SMM on renal injury in diabetic mice and its underlying mechanisms, focusing on its association with macrophage inflammaging. Results indicate that SMM suppresses macrophage inflammaging by modulating the ERK/NF-κB signaling pathway, thereby reversing DKD progression. These findings reveal novel functions of SMM and highlight its potential as a novel therapeutic strategy for DKD.

2. Materials and methods

2.1. Chemicals and drugs

Streptozotocin (STZ) was purchased from Sigma-Aldrich (S0130, USA). *S*-methylmethionine (SMM) was obtained from Tokyo Chemical Industry (M0644, Japan). FR 180204 was purchased from Ambeed (A867944, USA). Ceramide C6 was obtained from Santa Cruz (sc-3527, USA).

2.2. Animals

2.2.1. Animal housing and treatment

All animal experiments were conducted according to the protocol approved by the Animal Ethics Committee of West China Hospital of Stomatology, Sichuan University (No. WCHSIRB-D-2024-143). Five-week-old male C57BL/6J mice were purchased from GemPharmatech (Nanjing, China). All mice were maintained under specific pathogen-free (SPF) conditions at the State Key Laboratory of Oral Diseases, Sichuan University, with free access to food and water.

After acclimatization, control group (Ctrl, $n = 6$) mice were fed a standard chow diet, while the other mice received a high-fat diet (HFD). After 4 weeks, HFD-fed mice were injected intraperitoneally with STZ (50 mg/kg) for 5 consecutive days, while Ctrl mice received an equal volume of citrate buffer. Fasting blood glucose (FBG) was measured three days after the last STZ injection, and mice with FBG levels exceeding 11.1 mmol/L were considered diabetic mice. Diabetic mice were then randomly divided into three groups ($n = 6$): diabetes mellitus (DM) group, DM + SMM low-dose group (SMM-L), and DM + SMM high-dose group (SMM-H). The dosages of SMM were determined based on previous reports and our preliminary experiments. Mice in the low- and high-dose groups received 50 mg/kg and 100 mg/kg of SMM, respectively, by daily gavage for 10 weeks. The Ctrl and DM groups received an equal volume of double-distilled water. Body weight and FBG of mice were monitored weekly. Mice were euthanized by intraperitoneal injection of 1 % pentobarbital sodium followed by cervical dislocation, and blood and kidney samples were collected for subsequent analyses.

2.2.2. Insulin tolerance and glucose tolerance tests

During the final week of treatment, insulin tolerance and glucose tolerance tests were performed. After 8 h of fasting, mice were intraperitoneally injected with insulin (1 U/kg), and blood glucose levels were measured from the tail vein at 0, 15, 30, 60, and 120 min post-injection. For the glucose tolerance test, mice were fasted overnight and intraperitoneally injected with glucose (1.5 g/kg), and blood glucose was measured at 0, 15, 30, 60, and 120 min after glucose administration.

2.2.3. Histological staining

Kidney tissues were fixed in 4 % paraformaldehyde, embedded in paraffin, and sectioned at 4 μm. Hematoxylin and eosin (H&E), periodic acid–Schiff (PAS), and Masson's trichrome staining were performed to evaluate glomerular morphology, mesangial expansion, and fibrosis, respectively. Samples were scanned in high definition using VS200 (Olympus, Japan).

2.2.4. Serum collection and measurement

Mice blood samples were centrifuged at 3000 rpm for 15 min at 4 °C to obtain serum. Levels of blood urea nitrogen, serum creatinine, and uric acid were determined using commercial biochemical kits (Jianglai, Shanghai, China) following the manufacturer's instructions. Serum concentrations of cystatin C (Cys-C), kidney injury molecule-1 (KIM-1), interleukin-1β (IL-1β), IL-6, tumor necrosis factor-α (TNF-α), and IL-10 were quantified using commercial ELISA kits (Elabscience, Wuhan, China).

2.3. Cells

2.3.1. Cell culture and treatment

RAW 264.7 macrophages were provided by the State Key Laboratory of Oral Diseases, Sichuan University. Cells were cultured in DMEM medium (Gibco, USA) containing 10 % FBS (PAN-Seratech, Germany) and incubated at 37 °C in a humidified atmosphere with 5 % CO_2. The glucose concentration in the culture medium of the control group was maintained at 5.5 mM for 24 h. For the high-glucose (HG) group, cells were exposed to a high-glucose medium at a concentration of 33 mM for 24 h. In the SMM intervention groups, cells were pretreated with either 2 mM or 4 mM SMM for 1 h, and subsequently incubated under high-glucose conditions (33 mM) for 24 h. For the ERK inhibitor group, cells were pretreated with 10 μM FR 180204 for 1 h prior to being subjected to high-glucose (33 mM) exposure for 24 h. Similarly, in the ERK activator group, cells received a 1-h pretreatment with 10 μM Ceramide C6, followed by 24-h incubation in high-glucose (33 mM) medium. In the combination group of SMM and the ERK inhibitor, cells were co-pretreated with 4 mM SMM and 10 μM FR 180204 for 1 h, and then incubated under high-glucose conditions (33 mM) for 24 h. Likewise, in the combination group of SMM and the ERK activator, cells were co-pretreated with 4 mM SMM and 10 μM Ceramide C6 for 1 h, followed by 24-h exposure to high-glucose (33 mM) medium.

2.3.2. Cell viability assay

Cell viability of RAW 264.7 macrophages was assessed using the Cell Counting Kit-8 (CCK-8, K1018, APExBIO, USA) to determine the optimal concentration of SMM. Briefly, cells were seeded into 96-well plates and treated with different concentrations of SMM for 24 h. Subsequently, CCK-8 solution was added to the culture medium, and cells were incubated for another 2 h at 37 °C. Finally, absorbance at 450 nm was measured using a microplate reader.

2.3.3. Latex beads phagocytosis assay

Red fluorescent latex beads (L2778, Sigma-Aldrich, USA) were mixed with 1 % bovine serum albumin at a ratio of 1:100 and incubated at room temperature in the dark for 30 min, followed by ultrasonication for 5 min before use. RAW 264.7 cells (1×10^5 per well) were seeded in confocal dishes (NEST, China) and incubated with 2 mL of latex bead suspension at 37 °C for 1.5 h. After washing with PBS three times, samples were fixed with 4 % paraformaldehyde for 15 min, permeabilized with PBS containing 0.1 % Triton X-100 for 15 min. The cytoskeleton was stained with Actin-Tracker Green-488 (C2201S, Beyotime, China) at 37 °C for 20 min. After additional PBS washes, nuclei were counterstained with DAPI (P0131, Beyotime, China) for 10 min at 37 °C. Images of red fluorescent latex bead phagocytosis were captured using a FV3000 laser confocal microscope (Olympus, Japan).

2.3.4. Transwell migration assay

RAW 264.7 cells (1×10^5 per well) were suspended in serum-free high-glucose DMEM and seeded into the upper chamber of an 8 μm pore insert (3428, Corning) in a 6-well plate. Each lower chamber contained 1.5 mL of DMEM medium. After incubation for 24 h at 37 °C and 5 % CO_2, cells were fixed with 4 % paraformaldehyde and stained with 0.1 % crystal violet for 30 min at room temperature. Cells remaining on the upper surface of the membrane were removed with a cotton swab. After washing with PBS, migrated cells were observed and imaged under an IX73 microscope (Olympus, Japan).

2.3.5. Senescence-associated β-galactosidase (SA-β-gal) staining

SA-β-Gal staining was performed using a commercial kit (C0602, Beyotime, China) following the manufacturer's protocol. RAW 264.7 cells (1×10^5 per well) were fixed at room temperature for 15 min, followed by overnight incubation with staining solution at 37 °C. After washing with PBS, blue-stained senescent cells were observed and imaged using an IX73 microscope (Olympus, Japan).

2.3.6. Flow cytometry

RAW 264.7 cells were collected and adjusted to a concentration of 1×10^6 cells per testing tube. After centrifugation at 1000 rpm for 5 min, cells were resuspended in PBS. To block Fc receptor activity, cells were incubated on ice with CD16/CD32 antibody (156604, Biolegend, USA) for 20 min. Subsequently, cells were stained with PE anti-CD206 (25-2061-80, eBioscience, USA) and PE-Cyanine7 anti-CD86 (25-0862-80, eBioscience, USA) for 30 min at room temperature in the dark. After two washes, cells were resuspended in 500 μL PBS containing 2 % FBS and analyzed using a CytoFLEX S flow cytometer (Beckman, USA).

2.4. Real-time qPCR (RT-qPCR)

Total RNA was isolated from kidney tissues or RAW 264.7 cells using the Total RNA Isolation Kit (RC113-01, Vazyme, China) according to the manufacturer's protocol. Total RNA (1 mg) of each sample was reverse transcribed into cDNA using the 1st Strand cDNA Synthesis Kit (R211-01, Vazyme, China). RT-qPCR was performed with qPCR SYBR Green Master Mix (11201ES03, Yeasen, China) on an Applied Biosystems QuantStudio 3 Real-Time PCR System (Thermo Fisher, USA). Primer sequences used were provided in Supplemental material Table S1. Relative mRNA expression levels were calculated using the 2ˆ-ΔΔCT method, normalized to β-actin.

2.5. Immunofluorescence staining

For kidney tissue, sections were deparaffinized in xylene and rehydrated in ethanol. Antigen retrieval was performed using citrate buffer, followed by permeabilization in PBS containing 0.1 % Triton X-100 for 15 min. After washing with PBS, sections were blocked with 5 % bovine serum albumin for 30 min. The sections were then incubated overnight at 4 °C with primary antibodies against F4/80 (1:100, 14-4801-82, eBioscience, USA), CD86 (1:200, ER1906-01, Huabio, China), CD206 (1:200, HA722892, Huabio, China), and Phospho-ERK1/2 (1:200, ET1610-13, Huabio, China). After three washes, sections were incubated for 1 h at room temperature in the dark with FITC-conjugated goat anti-rabbit IgG (1:500, A0562, Beyotime, China) or Cy3-conjugated goat anti-rat IgG (1:500, A0507, Beyotime, China). Nuclei were counterstained with DAPI (P0131, Beyotime, China) for 10 min. The stained sections were scanned in high definition using VS200 (Olympus, Japan).

For cells cultured in confocal dishes, cells were fixed with 4 % paraformaldehyde for 15 min, permeabilized with PBS containing 0.1 % Triton X-100 for 15 min, and blocked with immunostaining blocking buffer (P0260, Beyotime, China) for 30 min. Cells were then incubated overnight at 4 °C with primary antibodies against IL-1β (1:100, HA601002, Huabio, China), IL-6 (1:200, 12912S, Cell Signaling Technology, USA), TNF-α (1:200, 11948S, Cell Signaling Technology, USA), p16 INK4A (1:200, YM8152, ImmunoWay, USA), p21 (1:200, 28248-1-AP, Proteintech, USA), Phospho-Histone H2A.X (1:200, YM8195, ImmunoWay, USA), Phospho-ERK1/2 (1:200, ET1610-13, Huabio, China), and Phospho-NF-κB p65 (1:200, 82335-1-RR, Proteintech, USA). After PBS washing, cells were incubated for 1 h in the dark with FITC-conjugated goat anti-mouse IgG (1:500, A0568, Beyotime, China), FITC-conjugated goat anti-rabbit IgG (1:500, A0562, Beyotime, China), or Cy3-conjugated goat anti-rabbit IgG (1:500, A0516, Beyotime, China). Nuclei were counterstained with DAPI for 10 min. The samples were imaged in high definition using FV3000 (Olympus, Japan).

2.6. Western blot

Cells or kidney tissues were lysed in RIPA lysis buffer (PC101, Epizyme Biotech, China) supplemented with a protease and phosphatase inhibitor cocktail (GRF103, Epizyme Biotech, China). Protein concentrations were determined using a BCA protein quantification kit (KTD3001, Abbkine, China). Equal amounts of protein samples were separated by sodium dodecyl sulfate - polyacrylamide gel

electrophoresis (SDS-PAGE) and transferred onto 0.45 μm polyvinylidene fluoride (PVDF) membranes (IPVH00010, Merck Millipore Ltd., Germany). The membranes were blocked with a commercial blocking buffer (PS108P, Epizyme Biotech, China) at room temperature for 30 min. After blocking, the membranes were incubated overnight at 4 °C with the following primary antibodies: β-actin (1:10000, EM21002, Huabio, China), IL-1β (1:1000, HA601002, Huabio, China), IL-6 (1:1000, 12912S, Cell Signaling Technology, USA), TNF-α (1:1000, 11948S, Cell Signaling Technology, USA), p16 INK4A (1:3000, YM8152, ImmunoWay, USA), p21 (1:2000, 28248-1-AP, Proteintech, USA), Phospho-Histone H2A.X (1:3000, YM8195, ImmunoWay, USA), ERK1/2 (1:5000, ET1601-29, Huabio, China), Phospho-ERK1/2 (1:5000, ET1610-13, Huabio, China), NF-κB p65 (1:2000, 10745-1-AP, Proteintech, USA), and Phospho-NF-κB p65 (1:2000, 82335-1-RR, Proteintech, USA). After extensive washing, the membranes were incubated for 1 h at room temperature with HRP-conjugated goat anti-mouse IgG secondary antibody (1:10000, HA1006, Huabio, China) or HRP-conjugated goat anti-rabbit IgG secondary antibody (1:10000, HA1001, Huabio, China). Protein bands were visualized using an enhanced chemiluminescence (P0018, Beyotime, China). Images were captured using the ChemiDoc™ MP Imaging System (734BR2136, Bio-Rad, USA).

2.7. Bioinformatics and network pharmacology analysis

2.7.1. Microarray dataset acquisition and identification of differentially expressed genes (DEGs)

The Gene Expression Omnibus (GEO) database was searched using diabetic kidney disease or diabetic nephropathy as keywords. Based on sample size and relevance, dataset GSE96804 was selected, including 41 diabetic kidney disease samples and 20 normal renal samples from nephrectomy tissues. Differentially expressed genes (DEGs) between DKD and control samples were identified using the limma package in R 4.2.3, with thresholds of $|\log_2 FC| > 1$ and $p < 0.05$. Volcano plots and heatmaps were visualized using the ggplot2 package and pHeatmap package.

2.7.2. Gene set enrichment analysis (GSEA) and gene set variation analysis (GSVA)

GSEA was performed based on identified DEGs to determine potential pathogenic pathways. GSVA, a non-parametric and unsupervised method, was applied using the GSVA package in R 4.2.3 to further evaluate pathway activity variations.

2.7.3. Potential targets of SMM in DKD

Potential targets of SMM were retrieved from CTD (https://ctdbase.org/), BATMAN-TCM (http://bionet.ncpsb.org.cn/batman-tcm/), and SwissTargetPrediction (http://www.swisstargetprediction.ch/). Disease-related targets of DKD were collected from GeneCards (https://www.genecards.org/), OMIM (https://omim.org/), DisGeNET (https://www.disgenet.org/), and Therapeutic Target Database (TTD, http://db.idrblab.net/ttd/). Additionally, DEGs identified from GSE96804 were included. Common target genes of SMM and DKD were determined using Venn diagram analysis.

2.7.4. Gene enrichment analysis

Common targets of SMM and DKD were analyzed for GO, KEGG, Reactome, and WikiPathways enrichment using the clusterProfiler package and org.Hs.eg.db package in R 4.2.3.

2.7.5. Protein–protein interaction (PPI) network

Common target genes of SMM and DKD were imported into the STRING database (https://string-db.org) to construct a PPI network for *Homo sapiens*, which was visualized using Cytoscape 3.8. The MCODE plugin in Cytoscape was used to analyze and identify key clusters and hub targets.

2.8. Statistical analysis

All quantitative data were obtained from at least three independent experiments. Statistical analyses were performed using GraphPad Prism 9.3.1 software. Comparisons between two groups were performed using unpaired Student's *t*-test, and comparisons among multiple groups were conducted using one-way ANOVA followed by Tukey's *post hoc* test. Data are presented as mean ± standard deviation (SD), and statistical significance was defined as $p < 0.05$.

3. Results

3.1. SMM improves glycemic control and preserves renal function in diabetic mice

To investigate the effects of *S*-methylmethionine (SMM) on renal function in diabetic mice, a streptozotocin-induced diabetic mouse model was established and treated with low or high doses of SMM for ten weeks (Fig. 1A). Body weight and blood glucose levels were monitored in all mice throughout the experiment. The diabetes mellitus (DM) group exhibited progressive weight loss and persistent hyperglycemia relative to the control (Ctrl) group, whereas SMM treatment mitigated these alterations in a dose-dependent manner (Fig. 1B, C and Fig. S1A, B). Furthermore, insulin tolerance tests (ITT) and glucose tolerance tests (GTT) consistently demonstrated that SMM treatment significantly improved glucose metabolism and insulin sensitivity in diabetic mice (Fig. 1D, E).

Histopathological analyses were performed using hematoxylin and eosin (H&E), periodic acid-Schiff (PAS), and Masson staining. Mice in the DM group exhibited severe renal pathological alterations, including glomerular hypertrophy, mesangial matrix expansion, and interstitial fibrosis. These pathological changes were significantly ameliorated by SMM treatment (Fig. 1F). Quantitative analysis confirmed that compared with the DM group, SMM-treated groups demonstrated dose-dependently reduced glomerular volume, mesangial expansion, and fibrotic area (Fig. 1G-I). Besides, compared with the Ctrl group, the DM group exhibited significantly elevated levels of blood urea nitrogen (BUN), serum creatinine (Scr), and uric acid, indicating renal dysfunction. SMM treatment notably improved these abnormal indicators, with the high-dose group showing superior efficacy (Fig. 1J-L). Collectively, these results demonstrated that SMM effectively improves glycemic control and preserves renal function in diabetic mice in a dose-dependent manner.

3.2. SMM attenuates inflammaging signatures in DKD

To investigate the potential mechanisms by which SMM participates in the regulation of DKD, we analyzed the Gene Expression Omnibus (GEO) dataset GSE96804 to identify differentially expressed genes (DEGs) associated with the disease. Differential expression analysis revealed a total of 650 DEGs ($|\log_2 FC| > 1$, $p < 0.05$), including 312 downregulated and 338 upregulated genes (Fig. 2A). To visualize the expression patterns of key genes, the top 100 DEGs were presented in a heat map (Fig. 2B). Gene set enrichment analysis (GSEA) showed significant enrichment of aging- and inflammation-related pathways in DKD, particularly the "RODWELL AGING KIDNEY UP" and "WP INFLAMMATORY RESPONSE PATHWAY" gene sets (Fig. 2C, D). Consistently, gene set variation analysis (GSVA) confirmed that both pathways were markedly upregulated in DKD samples compared with controls (Fig. 2E). Moreover, correlation analysis demonstrated that the activities of these pathways were strongly associated with well-established markers of kidney injury and fibrosis, including collagen type I alpha 2 (*COL1A2*), fibronectin 1 (*FN1*), and serpin family E member 1 (*SERPINE1*), supporting a close relationship between inflammaging processes and DKD progression (Fig. 2F).

We subsequently validated these findings in the diabetic mouse

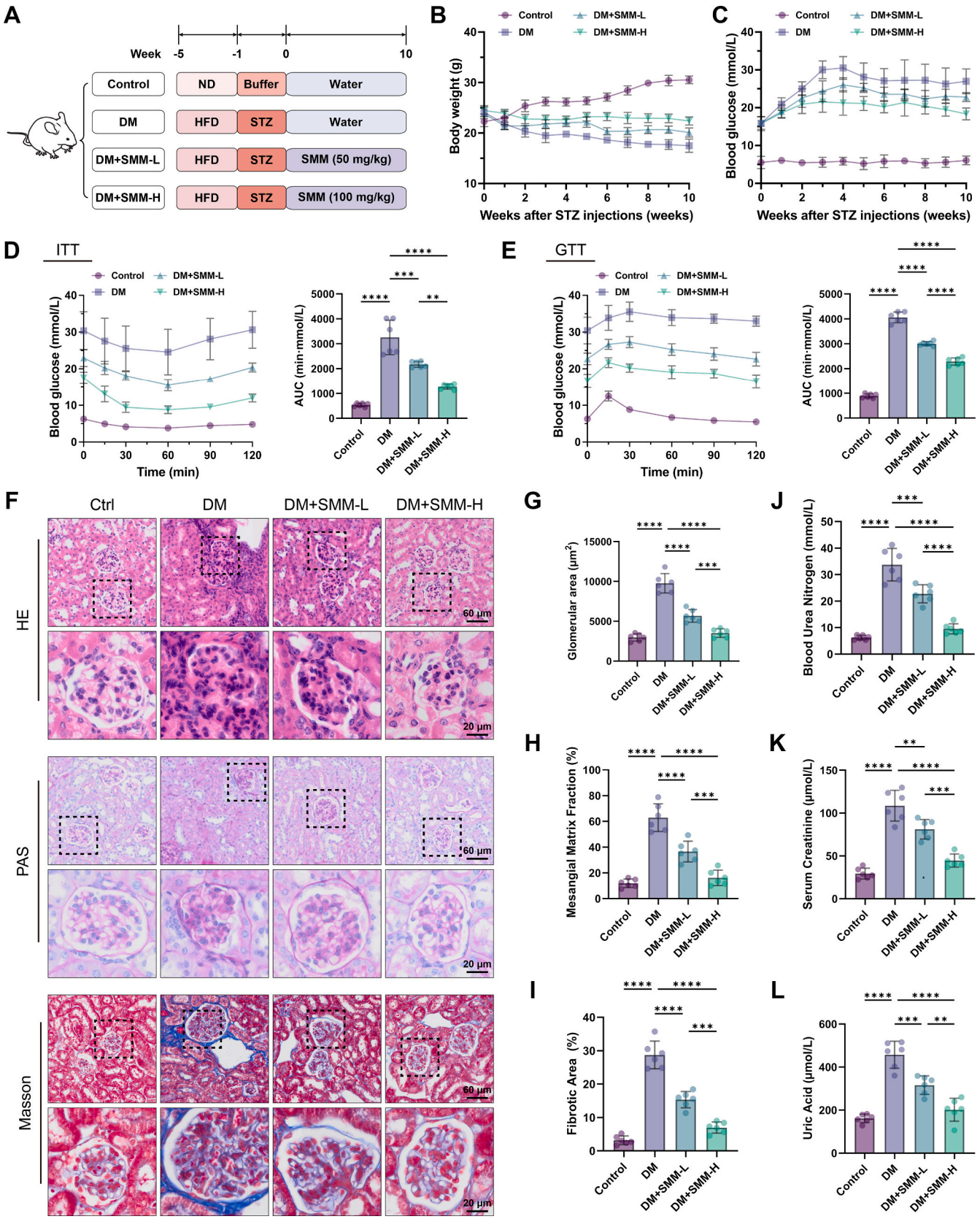

Fig. 1. SMM improves glycemic control and preserves renal function in diabetic mice.
(A) Schematic of animal groups and treatment regimen. (B) Changes in body weight during the treatment period, measured weekly. (C) Changes in blood glucose during the treatment period, measured weekly. (D) Insulin tolerance tests (ITT) results and AUC for ITT. (E) Glucose tolerance tests (GTT) results and AUC for GTT. (F) Representative hematoxylin and eosin (H&E), periodic acid-Schiff (PAS), and Masson staining of renal tissue. Scale bars, 60 μm and 20 μm. (G-I) The glomerular area, mesangial matrix fraction, and fibrotic area in each group. (J-L) Serum concentrations of blood urea nitrogen (BUN), serum creatinine (Scr), and uric acid. Data are presented as mean ± SD ($n = 6$). *$p < 0.05$, **$p < 0.01$, ***$p < 0.001$, ****$p < 0.0001$.

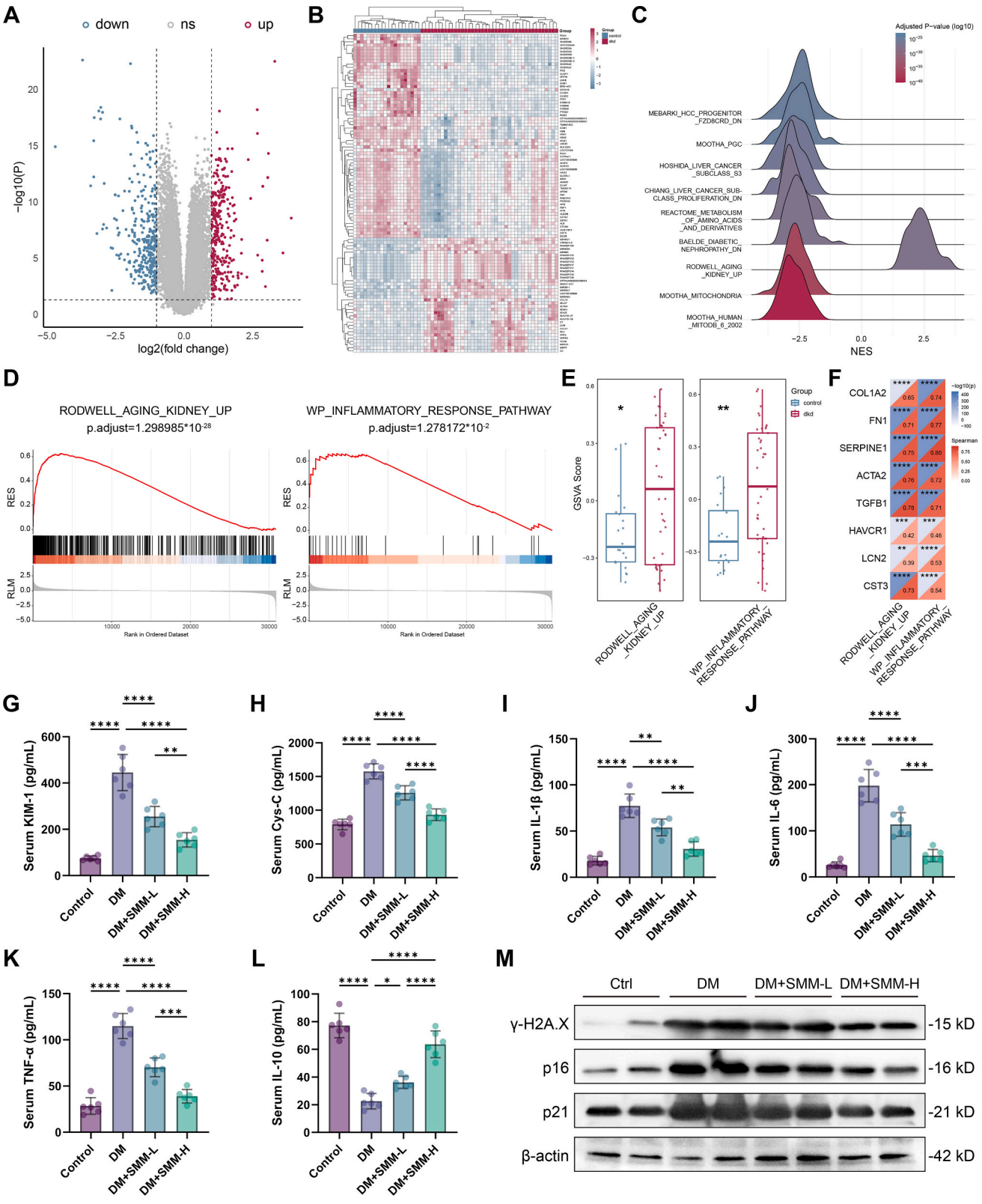

Fig. 2. SMM attenuates inflammaging signatures in DKD.

(A) Volcano plot of differentially expressed genes (DEGs) between DKD samples and normal kidney samples in GSE96804 dataset. (B) Heat map of the top 100 DEGs. (C) Ridgeline plot of genset enrichment analysis (GSEA). (D) GSEA of aging and inflammation related pathways. (E) Gene set variation analysis (GSVA) of aging and inflammation related pathways demonstrated by box plots. (F) The correlation analysis between the score of aging and inflammation related pathways based on GSVA and renal injury markers. (G-L) Serum concentrations of kidney injury molecule 1 (KIM-1), cystatin C (Cys-C), interleukin (IL)-1β, IL-6, tumor necrosis factor-α (TNF-α), and IL-10. (M) Representative γ-H2A.X, p16, and p21 bands by Western blot in mice kidneys. Data are presented as mean ± SD ($n = 6$). *$p < 0.05$, **$p < 0.01$, ***$p < 0.001$, ****$p < 0.0001$.

model. Enzyme-linked immunosorbent assay (ELISA) demonstrated that levels of kidney injury molecule 1 (KIM-1) and cystatin C (Cys-C) were markedly elevated in the DM group, indicating worsening renal injury, while SMM treatment significantly reduced their concentrations in a dose-dependent manner (Fig. 2G, H). In parallel, proinflammatory cytokines including interleukin (IL)-1β, IL-6, and tumor necrosis factor-α (TNF-α) were substantially increased in the DM group, reflecting a heightened inflammatory state. SMM supplementation effectively suppressed these cytokines, with the higher dose exerting a more pronounced effect (Fig. 2I-K). Conversely, the anti-inflammatory cytokine IL-10 was decreased in diabetic mice but restored by SMM, indicating an immunoregulatory shift (Fig. 2L). To further assess cellular senescence, we examined the expression of senescence-associated proteins in renal tissue. To comprehensively evaluate hyperglycemia-induced senescence, we selected γ-H2A.X, p16, and p21 as representative markers. Western blot analysis revealed significant upregulation of γ-H2A.X, p16, and p21 in the DM group. Strikingly, SMM treatment reduced the accumulation of these proteins, suggesting a protective role against diabetes-induced renal senescence (Fig. 2M and Fig. S2A-C).

Taken together, these results indicate that DKD is characterized by activation of inflammaging pathways, and that SMM attenuates renal injury by suppressing inflammatory cytokines production and reducing senescence-associated proteins levels.

3.3. SMM reprograms macrophage polarization to reduce renal inflammation in diabetic mice

To further explore the potential molecular targets of SMM in DKD, we integrated predicted pharmacological targets of SMM, known DKD-associated genes, and DEGs identified from patient transcriptomic data. Intersection analysis yielded 116 common targets (Fig. 3A). GO and WikiPathways enrichment analysis of these genes revealed strong associations with innate immune regulation, inflammatory signaling, and macrophage activation pathways, implicating macrophages as potential mediators of SMM's effects (Fig. 3B, C).

To validate these predictions *in vivo*, renal sections were subjected to immunofluorescence staining for assessing the localization and expression of macrophage markers. Results indicate that compared to the Ctrl group, the DM group exhibited increased infiltration of $F4/80^+$ $CD86^+$ cells (representing M1-type macrophages) alongside reduced $F4/80^+$ $CD206^+$ cells (representing M2-type macrophages), suggesting a shift in macrophage polarization toward a proinflammatory phenotype. SMM treatment significantly reversed these changes, promoting a reduction in M1-type macrophages while enhancing M2-type macrophage infiltration (Fig. 3D, E). In addition, the M1/M2 ratio was significantly elevated in the DM group compared to the Ctrl group, while SMM treatment effectively reduced this ratio, indicating that SMM can restore the balance between M1 and M2 macrophages in diabetic kidney disease (Fig. 3F). Consistently, qPCR analysis revealed that the expression of the M1 marker nitric oxide synthase 2 (*Nos2*) was significantly upregulated in kidney tissues of DM group compared to the Ctrl group, but was suppressed after SMM treatment. Conversely, expression of the hallmark M2 gene arginase-1 (*Arg1*) decreased in DM group kidneys, and was recovered by SMM treatment, with greater recovery in the high-dose group (Fig. S3A, B). These findings suggest that macrophages appear to be the critical regulatory target through which SMM alleviates diabetic kidney injury. SMM may mitigate renal inflammation and promote a more reparative immune microenvironment by reprogramming macrophage polarization.

3.4. SMM suppresses ERK/NF-κB signaling activation in diabetic kidneys

To further elucidate the signaling pathways involved in the regulation of DKD by SMM, Reactome enrichment analysis was performed on the 116 common targets. Results revealed that these targets were closely associated with inflammation and immune regulation-related pathways, such as the MAPK signaling pathway and the AP-1 family signaling pathway, consistent with the findings of previous WikiPathways enrichment analysis (Fig. 4A, B). Further analysis using the STRING database and Cytoscape software identified 27 hub genes, such as *MAPK1*, *MAPK3*, and *IL-1B* (Fig. 4C). These genes play a pivotal role in mediating the therapeutic effects of SMM on DKD. Additionally, KEGG enrichment analysis confirmed the significant enrichment of these hub genes in the MAPK signaling pathway (Fig. S4A, B). Collectively, these data highlight the potential role of MAPK and downstream NF-κB/AP-1 signaling pathway in SMM-mediated regulation of DKD.

Therefore, we examined extracellular signal-regulated kinase (ERK) and nuclear factor kappa B (NF-κB) activation *in vivo* to validate whether SMM regulates DKD by targeting the MAPK/NF-κB axis. Western blot results revealed that diabetes markedly activated the ERK/NF-κB pathway, with increased phosphorylation of ERK and NF-κB p65 in the DM group. SMM treatment significantly reduced the levels of phospho-ERK (p-ERK) and phospho-NF-κB p65 (p-p65) proteins (Fig. 4D and Fig. S4C, D). Immunofluorescence staining confirmed significant nuclear translocation and accumulation of p-ERK in $F4/80^+$ macrophages in the DM group. SMM treatment substantially reduced nuclear p-ERK intensity, with greater efficacy observed in the high-dose group (Fig. 4E). To assess downstream consequences of these pathways, we measured mRNA levels of genes classically regulated by ERK/NF-κB. Diabetic mice exhibited robust induction of inflammation- and aging-associated transcripts, including FBJ osteosarcoma oncogene (*Fos*), jun proto-oncogene (*Jun*), matrix metallopeptidase 9 (*Mmp9*), and prostaglandin-endoperoxide synthase 2 (*Ptgs2*). SMM treatment effectively suppressed these elevations, with the high-dose group showing the more notable inhibitory effect (Fig. 4F-I). These findings suggest that SMM attenuates diabetic kidney injury by suppressing the activation of the ERK/NF-κB signaling pathway in renal macrophages, thereby reducing the expression of inflammaging and tissue injury mediators.

3.5. SMM restores macrophage function under high glucose

To determine the exact effects and mechanisms of SMM on macrophages, we conducted further *in vitro* experiments on RAW264.7 cells. Concentrations of 0, 0.25, 0.5, 1, 2, 4, 8, 16, and 32 mmol/L SMM were applied to RAW264.7 cells (Fig. 5A). Results indicate that SMM significantly affects cell viability when the concentration reaches 8 mM, with no apparent cytotoxicity at lower doses (Fig. 5B). Accordingly, 2 mM and 4 mM were selected as low and high concentration doses for subsequent experiments (Fig. 5B).

To systematically evaluate the effects of high glucose levels and the protective role of SMM on macrophages, we assessed a series of key functional and phenotypic indicators. Fluorescent bead phagocytosis assays confirmed that high glucose stimulation suppressed macrophage phagocytic activity, while SMM significantly restored phagocytic function (Fig. 5C, D). Furthermore, transwell migration assays revealed that high glucose exposure suppressed macrophage chemotaxis capacity, which was effectively rescued by SMM supplementation (Fig. 5E, F). We next examined cellular senescence using senescence-associated β-galactosidase (β-gal) staining. High glucose markedly increased the proportion of β-gal-positive cells, indicating accelerated macrophage senescence. SMM treatment reduced senescent cell accumulation, with the higher concentration conferring stronger protection (Fig. 5G, H). Flow cytometry analysis of macrophage polarization further revealed that high glucose induced a shift toward a proinflammatory phenotype, characterized by increased $CD86^+$ cells and reduced $CD206^+$ cells. SMM treatment reversed this polarity imbalance (Fig. 5I, J). Further analysis revealed that the M1/M2 ratio was significantly increased in the HG group and markedly decreased following SMM treatment. This result aligns with the trends observed in macrophage function and inflammaging, suggesting that SMM can have a therapeutic effect by ameliorating the imbalance between M1 and M2 macrophages in diabetes (Fig. 5K). Collectively, these findings demonstrate that SMM effectively

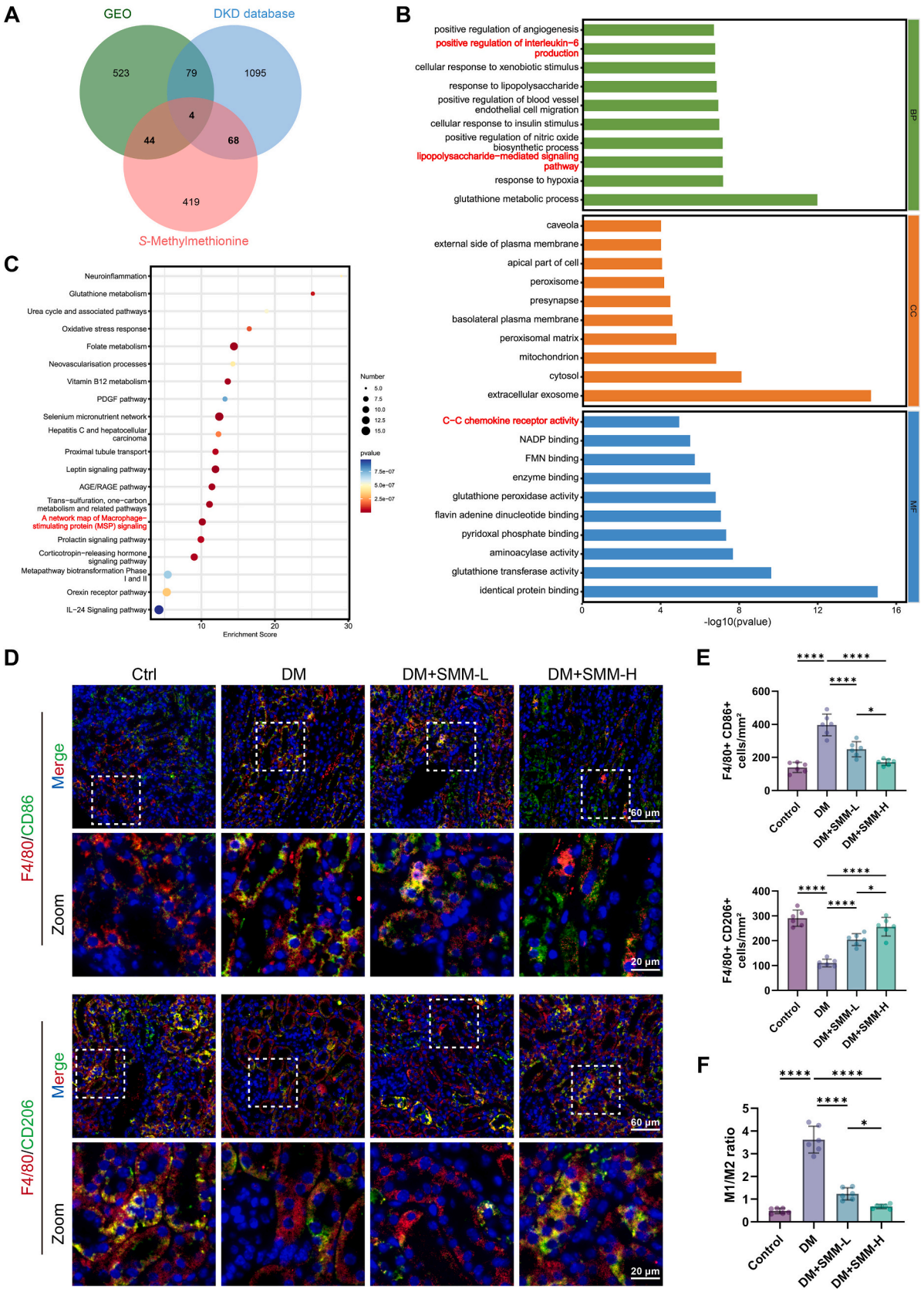

Fig. 3. SMM reprograms macrophage polarization to reduce renal inflammation in diabetic mice.
(A) Venn plot of common targets. (B, C) GO and WikiPathways enrichment analysis of common targets. (D) Representative immunofluorescence co-localization staining of F4/80 and CD86 or CD206 in mice kidneys. Scale bars, 60 μm and 20 μm. (E) Quantitation of F4/80$^+$ CD86$^+$ cells/mm^2 and F4/80$^+$ CD206$^+$ cells/mm^2 in mice kidneys. (F) Quantitation of the M1/M2 ratio (number of F4/80$^+$ CD86$^+$ cells/ number of F4/80$^+$ CD206$^+$ cells). Data are presented as mean ± SD (n = 6). *p < 0.05, **p < 0.01, ***p < 0.001, ****p < 0.0001.

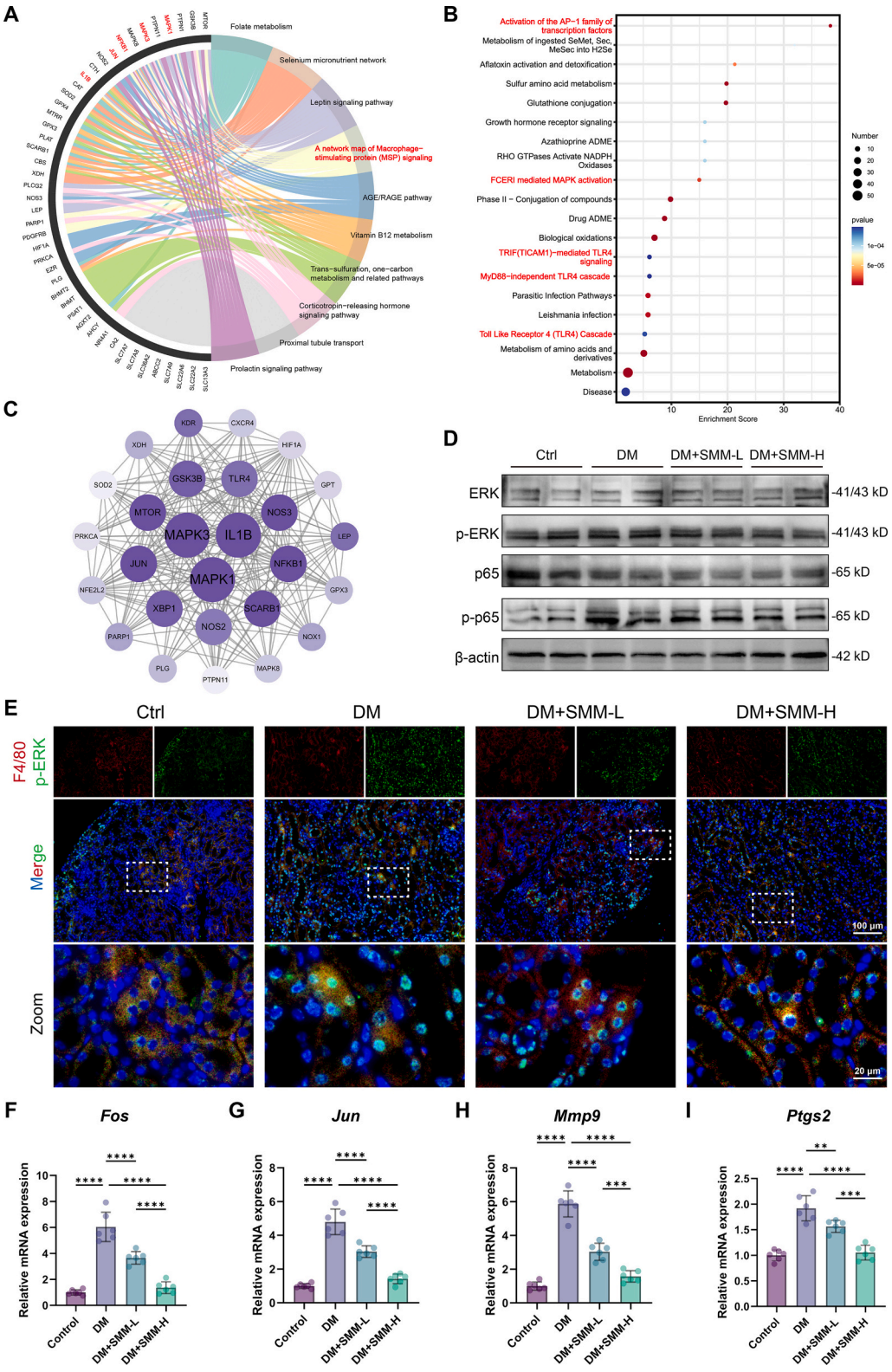

Fig. 4. SMM suppresses ERK/NF-κB signaling activation in diabetic kidneys.
(A, B) WikiPathways and Reactome enrichment analysis of common targets. (C) The PPI network of hub targets. (D) Representative extracellular signal-regulated kinase (ERK), phospho-ERK (p-ERK), nuclear factor kappa B (NF-κB) p65, and phospho-NF-κB p65 (p-p65) bands by Western blot in mice kidneys. (E) Representative immunofluorescence staining of F4/80 and p-ERK in mice kidneys. Scale bars, 100 μm and 20 μm. (F-I) Relative mRNA levels of FBJ osteosarcoma oncogene (*Fos*), jun proto-oncogene (*Jun*), matrix metallopeptidase 9 (*Mmp9*), and prostaglandin-endoperoxide synthase 2 (*Ptgs2*). Data are presented as mean ± SD ($n = 6$). *$p < 0.05$, **$p < 0.01$, ***$p < 0.001$, ****$p < 0.0001$.

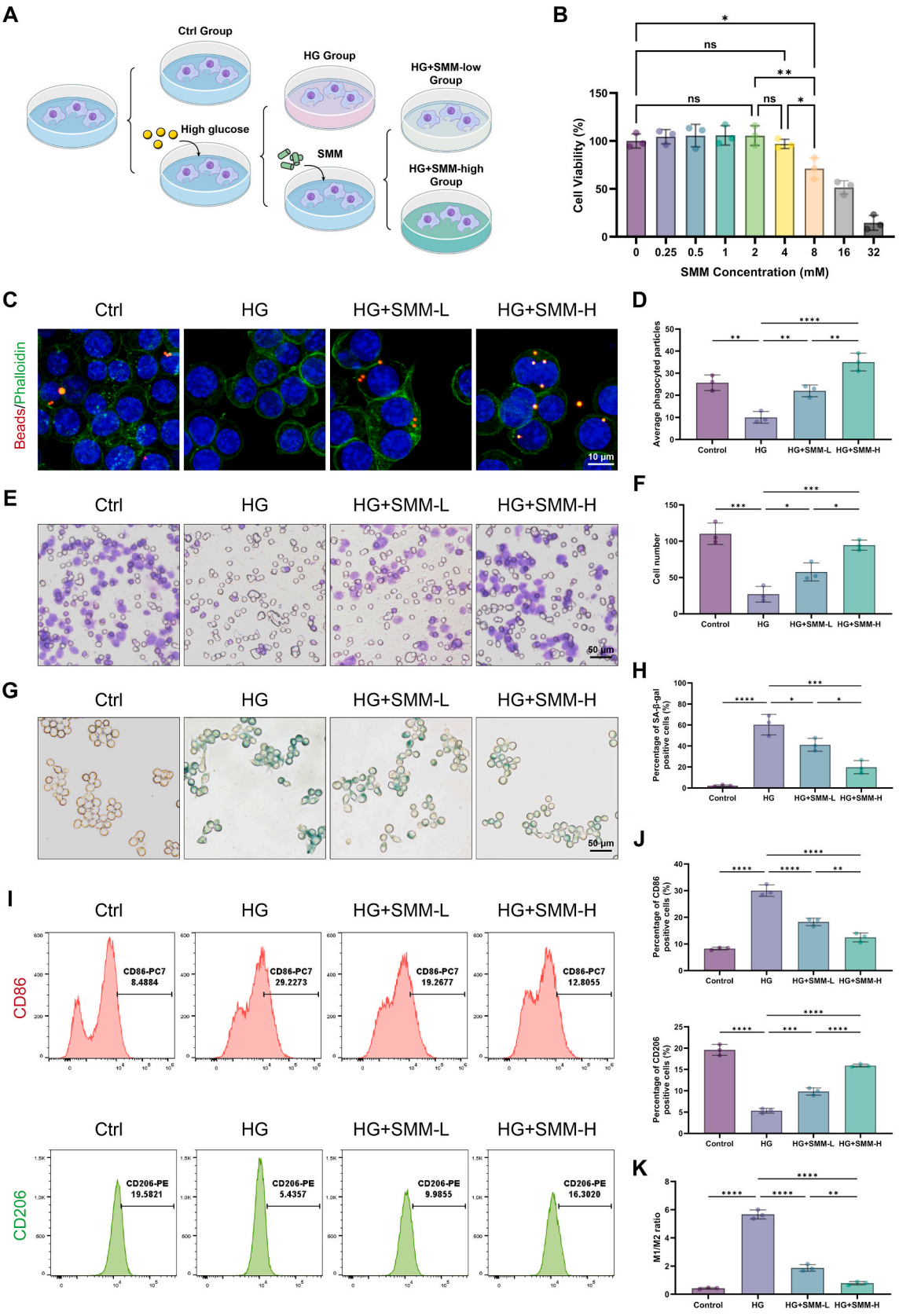

Fig. 5. SMM restores macrophage function under high glucose.
(A) Schematic illustration of the experimental group design. (B) CCK8 assay to determine the effect of different SMM concentrations on RAW264.7 cell viability. (C, D) Phagocytic function assessed by immunofluorescence. Scale bars, 10 μm. (E, F) Chemotaxis capability assessed by transwell migration assay. Scale bars, 50 μm. (G, H) Cellular senescence assessed by SA-β-gal staining. Scale bars, 50 μm. (I, J) Expressions of CD86 and CD206 marker assessed by flow cytometry. (K) Quantitation of the M1/M2 ratio. Data are presented as mean ± SD ($n = 3$). *$p < 0.05$, **$p < 0.01$, ***$p < 0.001$, ****$p < 0.0001$.

alleviates high glucose-induced macrophage dysfunction and phenotypic alterations by restoring phagocytic activity, enhancing chemotaxis capacity, suppressing cellular senescence, and rebalancing macrophage polarization.

3.6. SMM reduces inflammatory cytokines and senescence markers in macrophages under high glucose

To investigate the effects of SMM on high glucose-mediated inflammaging in macrophages, we evaluated inflammatory and senescence markers in RAW264.7 cells under high glucose treatment. Immunofluorescence analysis revealed robust induction of proinflammatory mediators, including IL-1β, IL-6, and TNF-α. SMM effectively reduced the expression of these cytokines (Fig. 6A, B). Furthermore, high glucose exposure led to prominent increases in nuclear p16, p21, and γ-H2A.X signals, which were attenuated by SMM (Fig. 6C, D). These findings were further supported by Western blot analysis, which demonstrated that SMM supplementation significantly reduced the expression of high glucose-induced inflammaging-related proteins (Fig. 6E, F and Fig. S5A-F). Given our prior analyses highlighting ERK/NF-κB signaling as a potentially key pathway, we next examined changes in ERK and p65 activation. High glucose stimulation markedly increased the levels of phosphorylated ERK (p-ERK) and phosphorylated p65 (p-p65), whereas treatment with SMM effectively suppressed this activation (Fig. 6G and Fig. S5G, H).

3.7. SMM exerts protective effects through modulation of the ERK/NF-κB signaling pathway

To establish whether ERK/NF-κB signaling mediates the protective effects of SMM, we employed the ERK inhibitor FR 180204 and the ERK activator Ceramide C6 in following studies. Immunofluorescence staining revealed that high glucose stimulation significantly increased the nuclear accumulation of p-ERK and p-p65, indicating pathway activation. Treatment with SMM reproduced suppression of these signals similar to that achieved by FR 180204. Moreover, combined treatment with SMM and ERK inhibitor did not provide additional suppression, suggesting convergent targeting of the same pathway. In contrast, treatment with the ERK activator further increased the levels of phosphorylated ERK (p-ERK) and phosphorylated p65 (p-p65), whereas co-treatment with SMM partially attenuated these effects (Fig. 7A-C). These observations were further confirmed by Western blot analysis (Fig. 7D and Fig. S6A, B).

Subsequently, alterations in downstream pathways of the ERK/NF-κB signaling axis were examined. In RAW264.7 cells, high glucose-induced increases in *Fos*, *Jun*, *Mmp9*, and *Ptgs2* expression were effectively suppressed by SMM treatment. Co-treatment with Ceramide C6 abrogated the suppression (Fig. 7E-H). Ceramide C6 also eliminated the SMM-mediated reduction in inflammaing-related protein levels (Fig. 7I, J and Fig. S6C-H). Furthermore, we investigated the effects of inhibiting the ERK/NF-κB signaling axis on macrophage senescence. Immunofluorescence and SA-β-gal staining revealed that treatment with the ERK inhibitor FR 180204 significantly alleviated senescence in high-glucose-exposed RAW264.7 cells, with similar results obtained in the SMM-treated group (Fig. S7A-D). The altered levels of aging-related markers such as p16, p21, and γ-H2A.X correlated with the activation levels of the ERK/NF-κB signaling, suggesting that SMM could effectively improve macrophage senescence by suppressing ERK/NF-κB pathway. Collectively, these results indicate that SMM alleviates macrophage inflammaing under diabetic conditions by inhibiting the ERK/NF-κB signaling axis.

4. Discussion

DKD is one of the most common and severe complications of diabetes, posing a heavy burden on global health [4]. With the increasing prevalence of DKD, growing attention has been directed toward understanding its molecular mechanisms and identifying potential therapeutic targets [31]. *S*-methylmethionine (SMM), also known as Vitamin U, is a naturally-derived amino acid derivative commonly found in vegetables such as cabbage, kale, spinach and garlic [29]. SMM displays a wide range of biological activities, including anti-inflammatory, anti-ulcer, antihyperlipidemic, and cytoprotective effects. In various disease models, SMM has been shown to possess potent free radical scavenging and antioxidant properties [28,30]. In this study, we discovered a novel therapeutic role of SMM in ameliorating diabetic renal injury. Diabetic mice treated with SMM showed improved metabolic disturbances, less weight loss, and lower hyperglycemic levels. Furthermore, pathological alterations of the kidney, such as glomerular hypertrophy, mesangial expansion, thickened basement membranes, and interstitial fibrosis, are characteristic features of DKD [32]. Our findings demonstrated that SMM significantly reversed these pathological changes and mitigated renal functional impairment.

Inflammaging has recently received wide attention as an important driver of persistent complications in metabolic disease [9]. Hyperglycemia triggers systemic chronic inflammation and promotes premature senescence in local cells *via* excessive inflammatory cytokines [12]. Senescent cells secrete the SASP in turn, which sustains inflammation and drives disease progression. Transcriptomic analysis of DKD patient dataset revealed significant enrichment of inflammation and senescence related pathways, which correlated strongly with renal injury. Targeting inflammaging may therefore represent a promising therapeutic strategy to intervene in DKD. In our experiments, SMM treatment markedly reduced serum levels of proinflammatory cytokines including IL-1β, IL-6 and TNF-α. SMM also lowered the expression of senescence associated proteins such as p16 and p21. These data indicate that SMM can effectively suppress inflammation and attenuate cellular senescence in the diabetic setting.

Macrophages are central innate immune cells in the diabetic kidney [16,33]. Two major macrophage phenotypes, M1 and M2, exert opposite effects in DKD. M1 macrophages accumulate in diabetic kidneys and release proinflammatory mediators that promote tissue injury [34]. M2 macrophages are associated with anti-inflammatory responses and tissue repair. Regulation of macrophage polarization has been shown to improve DKD outcomes [35,36]. In our study, diabetic mice displayed marked renal macrophage infiltration and a shift toward the proinflammatory M1 phenotype, exhibiting a significantly elevated M1/M2 ratio. SMM treatment restored macrophage polarization balance , promoted phenotype conversion from M1 toward M2 and reduced the M1/M2 ratio. Moreover, previous studies have indicated that diabetic macrophages exhibit functional impairments, including reduced phagocytic and migratory capacities, which can perpetuate excessive inflammation [37,38]. *In vitro*, SMM reversed these dysfunctions in RAW264.7 macrophages in a dose dependent manner. These results support the idea that the protective effects of SMM are closely linked to its capacity to modulate macrophage phenotype and function.

To further elucidate the underlying molecular mechanisms, we integrated network pharmacology and bioinformatics analyses. The results suggested that the ERK/NF-κB signaling pathway may play a critical role in SMM-mediated protection against DKD. ERK, a key member of the MAPK family, participates in signaling processes related to metabolism and inflammation [39]. Our data showed that ERK phosphorylation was significantly increased in diabetic kidneys and high glucose-stimulated macrophages, whereas SMM treatment effectively reduced phosphorylated ERK expression. NF-κB is a master transcription factor that regulates inflammatory and senescence networks, which has been reported to driving DKD progression [40,41]. SMM reversed high glucose induced NF-κB phosphorylation and nuclear translocation. These findings suggest that SMM exerts its protective effect by suppressing ERK/NF-κB signaling. To validate this mechanism, we further employed the ERK inhibitor FR180204 and the ERK activator Ceramide C6 [42,43]. Consistent with SMM treatment, FR180204

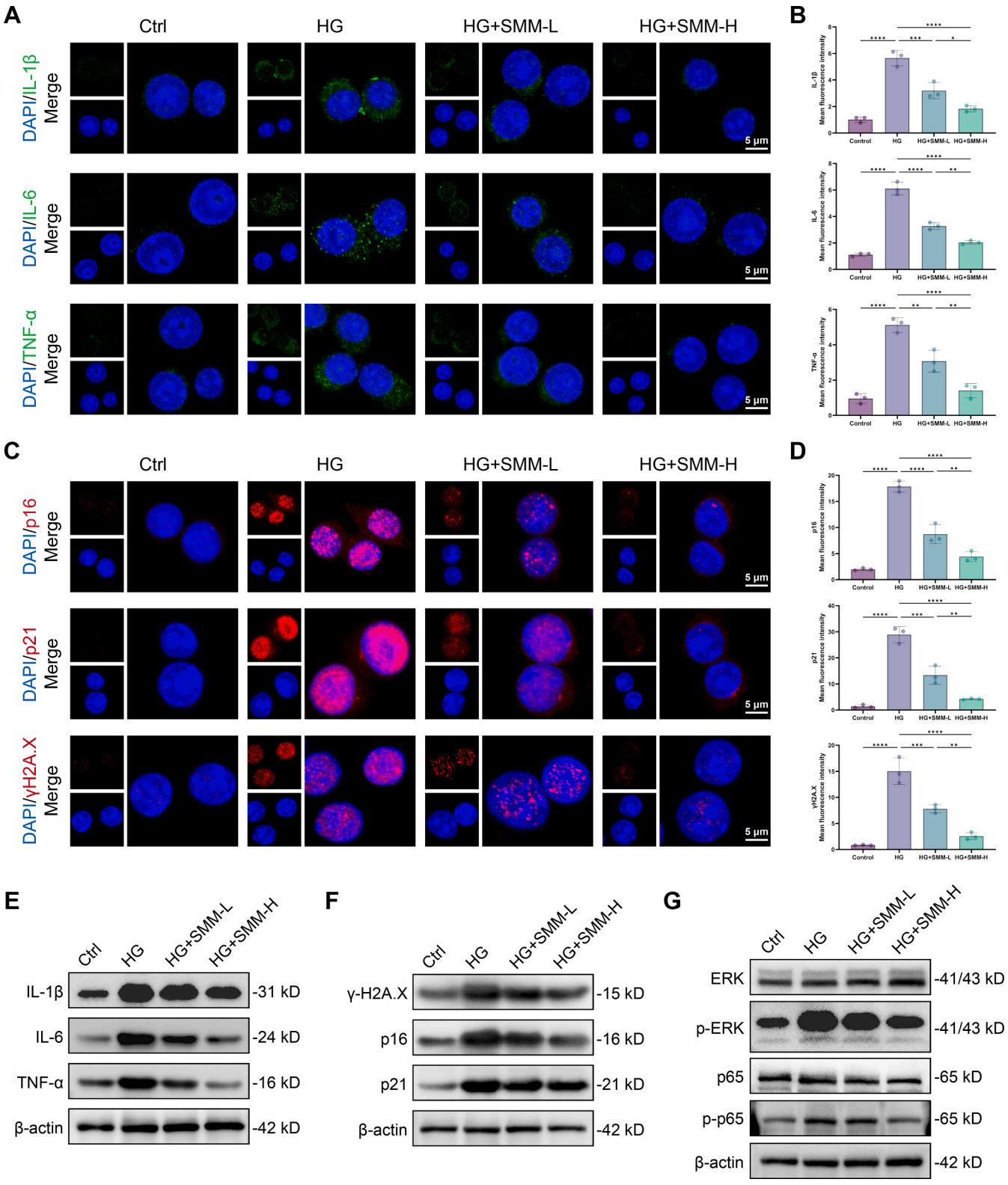

Fig. 6. SMM reduces inflammatory cytokines and senescences marker in macrophages under high glucose.
(A, B) Representative immunofluorescence staining and quantitative analysis of IL-1β, IL-6, and TNF-α in RAW264.7 cells. (C, D) Representative immunofluorescence staining and quantitative analysis of p16, p21, and γ-H2A.X in RAW264.7 cells. (E) Representative IL-1β, IL-6, and TNF-α bands by Western blot. (F) Representative p16, p21, and γ-H2A.X bands by Western blot. (G) Representative ERK, p-ERK, p65 and p-p65 bands by Western blot. Data are presented as mean ± SD ($n = 3$). *$p < 0.05$, **$p < 0.01$, ***$p < 0.001$, ****$p < 0.0001$.

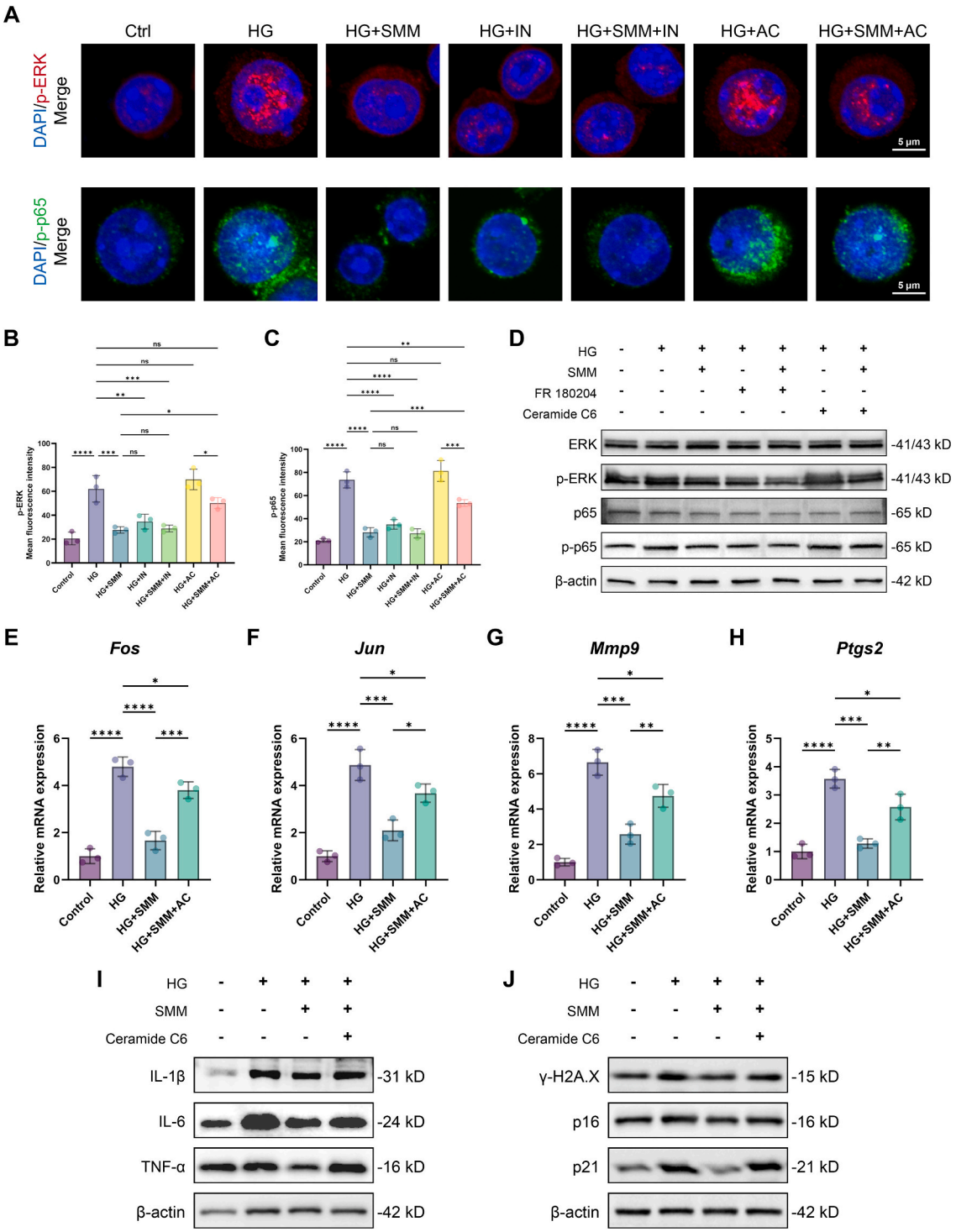

Fig. 7. SMM exerts protective effects through modulation of the ERK/NF-κB signaling pathway.
(A-C) Representative immunofluorescence staining and quantitative analysis of p-ERK and p-p65 in RAW264.7 cells. (D) Representative ERK, p-ERK, p65 and p-p65 bands by Western blot. (E-H) Relative mRNA levels of *Fos*, *Jun*, *Mmp9*, and *Ptgs2*. (I) Representative IL-1β, IL-6, and TNF-α bands by Western blot. (J) Representative p16, p21, and γ-H2A.X bands by Western blot. Data are presented as mean ± SD ($n = 3$). $^{*}p < 0.05$, $^{**}p < 0.01$, $^{***}p < 0.001$, $^{****}p < 0.0001$.

effectively inhibited ERK and NF-κB activation and downregulated the expression of downstream inflammatory and senescence-associated markers. Co-administration of SMM and FR180204 did not yield additional effects, whereas the ERK activator Ceramide C6 partially abolished the protective actions of SMM. Collectively, these results highlight the central role of ERK/NF-κB signaling in mediating the anti-inflammaging effects of SMM.

Current findings reveal that SMM acts as a negative regulator of the ERK/NF-κB pathway in macrophages, with ERK/NF-κB serving as the core signaling module targeted by SMM in diabetic kidney disease-associated macrophage inflammaging. Future studies should further investigate the upstream mechanisms underlying SMM-mediated ERK/NF-κB pathway alterations to elucidate potential targets of SMM regulation. It was shown that SMM functions as a methyl donor utilized by

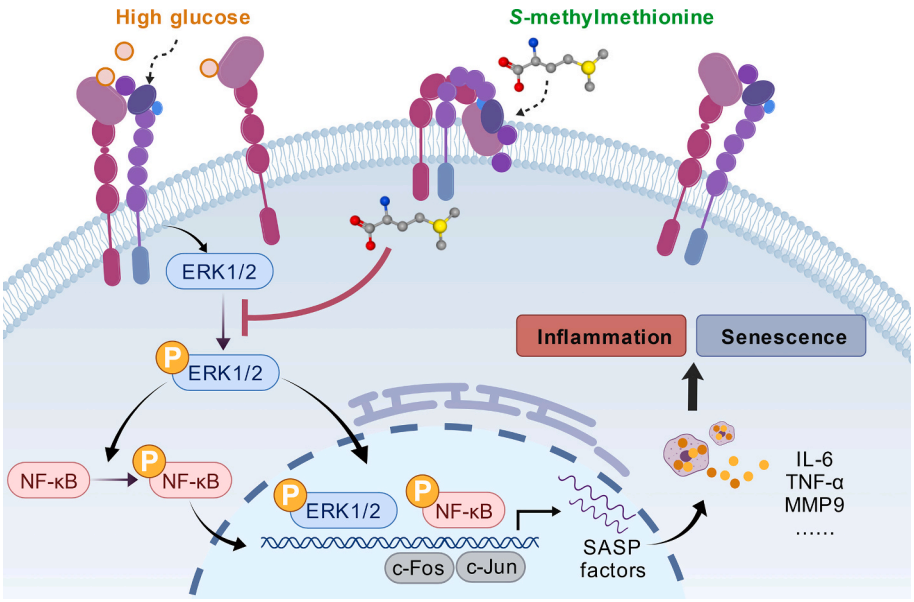

Fig. 8. SMM ameliorates renal injury in diabetic mice by modulating macrophage inflammaging *via* inhibiting the ERK/NF-κB signaling pathway (created with BioGDP.com).

betaine-homocysteine *S*-methyltransferase 2 (BHMT2) in one-carbon metabolism and the methionine cycle [44]. Through this pathway, SMM mediates the conversion of homocysteine (Hcy) to methionine (Met) and elevates the ratio of S-adenosylmethionine (SAM) to S-adenosylhomocysteine (SAH) [45,46]. Elevated Hcy levels are known to enable cascade activation of ERK signaling through multiple routes. Hcy can enhance the activity of Ras, a key upstream regulator in the Raf/MEK/ERK pathway, thereby initiating the cascade reaction [47]. Robert K et al. showed that cyclic AMP-dependent protein kinase (PKA) and phospholipid-dependent protein kinase (PKC) participate in Hcy-mediated ERK activation in mouse hippocampus [48]. In macrophages, excessive Hcy has also been reported to activate ERK/NF-κB-associated inflammatory responses through P2X7 receptor-dependent signaling, while Ca^{2+}-responsive pathways involving kinases such as Pyk2 and Src-family members represent additional mechanisms by which Hcy can potentiate ERK activation [49,50]. Meanwhile, SMM also exhibits the potential to regulate methylation levels through one-carbon metabolism, thereby altering the expression or activation state of related upstream regulatory proteins. Our future research will integrate metabolomics to investigate alterations in BHMT2-related one-carbon metabolism under hyperglycemia, while assessing the activity and epigenetic modification status of key target proteins such as Ras, PKA, PKC, as well as Ca^{2+}-responsive kinases, to explore their potential linkages with SMM.

Despite these advances, our study has several limitations. Findings are primarily derived from mouse models and RAW264.7 macrophages, so it remains to be clarified whether these observations can be extrapolated to human diabetic nephropathy. Furthermore, while our data suggest SMM exhibits protective effects under hyperglycemic and inflammatory conditions, its optimal dosing regimen, pharmacokinetic profile, tissue distribution, and metabolic outcomes in chronic metabolic diseases remain insufficiently characterized. Long-term and systematic evaluations are required to validate its therapeutic potential.

In summary, our results demonstrate that SMM ameliorates diabetic kidney injury by modulating macrophage inflammaging through suppression of the ERK/NF-κB signaling pathway (Fig. 8). To our knowledge, this is the first report identifying SMM as a novel regulator of macrophage inflammaging in DKD, providing new insights for the development of dietary or pharmacological interventions against diabetic complications.

CRediT authorship contribution statement

Hao Dong: Writing – review & editing, Writing – original draft, Visualization, Validation, Project administration, Methodology, Investigation, Formal analysis, Data curation, Conceptualization. **Linjie Shen:** Writing – original draft, Validation, Methodology, Investigation, Data curation. **Pawuziya Abulizi:** Visualization, Methodology, Investigation, Formal analysis. **Yuezhang Sun:** Validation, Methodology, Investigation. **Lulingxiao Nie:** Methodology, Investigation. **Aimin Cui:** Methodology, Investigation. **Qian Fu:** Investigation, Data curation. **Ning Ji:** Methodology, Investigation. **Yuwen Luo:** Validation, Investigation. **Chienshan Chen:** Resources, Conceptualization. **Aimin Xu:** Formal analysis, Conceptualization. **Wai Keung Leung:** Writing – review & editing, Writing – original draft, Supervision, Resources, Formal analysis, Conceptualization. **Qi Wang:** Writing – review & editing, Writing – original draft, Supervision, Resources, Project administration, Methodology, Funding acquisition, Conceptualization.

Funding

This work was supported by the National Natural Science Foundation of China (82470985 to Qi Wang), the Independent Research Project of the State Key Laboratory of Oral Diseases, West China Hospital of Stomatology, Sichuan University (SKLOD-2025RD009 to Qi Wang), and a grant from the Research Grants Council of the Hong Kong Special Administrative Region, China (17116819 to Wai Keung Leung).

Declaration of competing interest

The authors declare that they have no known competing financial interests or personal relationships that could have appeared to influence the work reported in this paper.

Appendix A. Supplementary data

Supplementary data to this article can be found online at https://doi.org/10.1016/j.intimp.2025.116038.

Data availability

Data will be made available on request.

References

[1] K.R. Tuttle, G.L. Bakris, R.W. Bilous, J.L. Chiang, I.H. de Boer, J. Goldstein-Fuchs, I. B. Hirsch, K. Kalantar-Zadeh, A.S. Narva, S.D. Navaneethan, J.J. Neumiller, U. D. Patel, R.E. Ratner, A.T. Whaley-Connell, M.E. Molitch, Diabetic kidney disease: a report from an ADA consensus conference, Am. J. Kidney Dis. 64 (2014) 510–533, https://doi.org/10.1053/j.ajkd.2014.08.001.

[2] M. Afkarian, L.R. Zelnick, Y.N. Hall, P.J. Heagerty, K. Tuttle, N.S. Weiss, I.H. de Boer, Clinical manifestations of kidney disease among US adults with diabetes, 1988-2014, Jama 316 (2016) 602–610, https://doi.org/10.1001/jama.2016.10924.

[3] H.J. Anders, T.B. Huber, B. Isermann, M. Schiffer, CKD in diabetes: diabetic kidney disease versus nondiabetic kidney disease, Nat. Rev. Nephrol. 14 (2018) 361–377, https://doi.org/10.1038/s41581-018-0001-y.

[4] K.R. Tuttle, R. Agarwal, C.E. Alpers, G.L. Bakris, F.C. Brosius, P. Kolkhof, J. Uribarri, Molecular mechanisms and therapeutic targets for diabetic kidney disease, Kidney Int. 102 (2022) 248–260, https://doi.org/10.1016/j.kint.2022.05.012.

[5] K. Watanabe, E. Sato, E. Mishima, M. Miyazaki, T. Tanaka, What's new in the molecular mechanisms of diabetic kidney disease: recent advances, Int. J. Mol. Sci. 24 (2022), https://doi.org/10.3390/ijms24010570.

[6] M.V. Perez-Gomez, M.D. Sanchez-Niño, A.B. Sanz, C. Martín-Cleary, M. Ruiz-Ortega, J. Egido, J.F. Navarro-González, A. Ortiz, B. Fernandez-Fernandez, Horizon 2020 In diabetic kidney disease: the clinical trial pipeline for add-on therapies on top of renin angiotensin system blockade, J. Clin. Med. 4 (2015) 1325–1347. https://doi.org/10.3390/jcm4061325.

[7] F. Ismail-Beigi, T. Craven, M.A. Banerji, J. Basile, J. Calles, R.M. Cohen, R. Cuddihy, W.C. Cushman, S. Genuth, R.H. Grimm Jr., B.P. Hamilton, B. Hoogwerf, D. Karl, L. Katz, A. Krikorian, P. O'Connor, R. Pop-Busui, U. Schubart, D. Simmons, H. Taylor, A. Thomas, D. Weiss, I. Hramiak, Effect of intensive treatment of hyperglycaemia on microvascular outcomes in type 2 diabetes: an analysis of the ACCORD randomised trial, Lancet 376 (2010) 419–430, https://doi.org/10.1016/s0140-6736(10)60576-4.

[8] A. Ajoolabady, D. Pratico, D. Tang, S. Zhou, C. Franceschi, J. Ren, Immunosenescence and inflammaging: mechanisms and role in diseases, Ageing Res. Rev. 101 (2024) 102540, https://doi.org/10.1016/j.arr.2024.102540.

[9] F. Prattichizzo, V. De Nigris, R. Spiga, E. Mancuso, L. La Sala, R. Antonicelli, R. Testa, A.D. Procopio, F. Olivieri, A. Ceriello, Inflammageing and metaflammation: the yin and yang of type 2 diabetes, Ageing Res. Rev. 41 (2018) 1–17, https://doi.org/10.1016/j.arr.2017.10.003.

[10] Q. Wang, L. Nie, P. Zhao, X. Zhou, Y. Ding, Q. Chen, Q. Wang, Diabetes fuels periodontal lesions via GLUT1-driven macrophage inflammaging, Int. J. Oral Sci. 13 (2021) 11, https://doi.org/10.1038/s41368-021-00116-6.

[11] R. Tang, Y. Ren, Y. Zhang, M. Yin, X. Ren, Q. Zhu, C. Gao, W. Zhang, G. Liu, B. Liu, Glucose-driven transformable complex eliminates biofilm and alleviates inflammaging for diabetic periodontitis therapy, Mater Today Bio 20 (2023) 100678, https://doi.org/10.1016/j.mtbio.2023.100678.

[12] C. Franceschi, P. Garagnani, P. Parini, C. Giuliani, A. Santoro, Inflammaging: a new immune-metabolic viewpoint for age-related diseases, Nat. Rev. Endocrinol. 14 (2018) 576–590, https://doi.org/10.1038/s41574-018-0059-4.

[13] I.M. Rea, D.S. Gibson, V. McGilligan, S.E. McNerlan, H.D. Alexander, O.A. Ross, Age and age-related diseases: role of inflammation triggers and cytokines, Front. Immunol. 9 (2018) 586, https://doi.org/10.3389/fimmu.2018.00586.

[14] C. Franceschi, P. Garagnani, G. Vitale, M. Capri, S. Salvioli, Inflammaging and 'Garb-aging', Trends Endocrinol. Metab. 28 (2017) 199–212, https://doi.org/10.1016/j.tem.2016.09.005.

[15] H. Zhao, J. Guo, Macrophages in focus: key drivers and therapeutic opportunities in diabetic kidney disease, Int. J. Biol. Sci. 21 (2025) 4647–4662, https://doi.org/10.7150/ijbs.112737.

[16] N. Youssef, M.H. Noureldein, M.E. Riachi, A. Haddad, A.A. Eid, Macrophage polarization and signaling in diabetic kidney disease: a catalyst for disease progression, Am. J. Physiol. Renal Physiol. 326 (2024) F301–f312, https://doi.org/10.1152/ajprenal.00266.2023.

[17] H. Ding, Q. Zhang, R. Yang, L. Fu, H. Jiang, Q. Zhu, S. Tai, Aberrant STING activation promotes macrophage senescence by suppressing autophagy in vascular aging from diabetes, iScience 28 (2025) 111594, https://doi.org/10.1016/j.isci.2024.111594.

[18] X. Ge, S. Wang, Z. Li, J. Yu, B. Liu, R. Wang, S. Bu, N. Wan, Y. Wang, C. Dai, Y. Lin, Lactate-activated GPR132-Src signal induces macrophage senescence and aggravates atherosclerosis under diabetes, Adv Sci (Weinh) 12 (2025) e00141, https://doi.org/10.1002/advs.202500141.

[19] Q. Li, P. Wang, Y. Gong, M. Xu, M. Wang, R. Luan, J. Liu, X. Li, Y. Shao, α-Klotho prevents diabetic retinopathy by reversing the senescence of macrophages, Cell Commun. Signal 22 (2024) 449, https://doi.org/10.1186/s12964-024-01838-w.

[20] L. Tao, S. Wu, Q. Wang, Z. Xi, Y. Zou, M. Cao, K. Liang, W. Xu, Q. Hu, Y. Ge, Z. Yin, Z. Ju, Z. Liu, IL-27 accelerates diabetic wound healing by modulating macrophage polarization, Int. Immunopharmacol. 155 (2025) 114575, https://doi.org/10.1016/j.intimp.2025.114575.

[21] M. Zhang, Z. Yan, L. Bu, C. An, D. Wang, X. Liu, J. Zhang, W. Yang, B. Deng, J. Xie, B. Zhang, Rapeseed protein-derived antioxidant peptide RAP alleviates renal fibrosis through MAPK/NF-κB signaling pathways in diabetic nephropathy, Drug Des. Devel. Ther. 12 (2018) 1255–1268, https://doi.org/10.2147/dddt.S162288.

[22] C. Yu, Z. Li, C. Nie, L. Chang, T. Jiang, Targeting Src homology phosphatase 2 ameliorates mouse diabetic nephropathy by attenuating ERK/NF-κB pathway-mediated renal inflammation, Cell Commun. Signal 21 (2023) 362, https://doi.org/10.1186/s12964-023-01394-9.

[23] X. Han, J. Wei, R. Zheng, Y. Tu, M. Wang, L. Chen, Z. Xu, L. Zheng, C. Zheng, Q. Shi, H. Ying, G. Liang, Macrophage SHP2 deficiency alleviates diabetic nephropathy via suppression of MAPK/NF-κB- dependent inflammation, Diabetes 73 (2024) 780–796, https://doi.org/10.2337/db23-0700.

[24] J.S. Arthur, S.C. Ley, Mitogen-activated protein kinases in innate immunity, Nat. Rev. Immunol. 13 (2013) 679–692, https://doi.org/10.1038/nri3495.

[25] K. Zhang, M. Li, K. Yin, M. Wang, Q. Dong, Z. Miao, Y. Guan, Q. Wu, Y. Zhou, Hyperoside mediates protection from diabetes kidney disease by regulating ROS-ERK signaling pathway and pyroptosis, Phytother. Res. 37 (2023) 5871–5882, https://doi.org/10.1002/ptr.7993.

[26] Y. Tian, H. Li, T. Qiu, J. Dai, Y. Zhang, J. Chen, H. Cai, Loss of PTEN induces lung fibrosis via alveolar epithelial cell senescence depending on NF-κB activation, Aging Cell 18 (2019) e12858, https://doi.org/10.1111/acel.12858.

[27] D. Topaloglu, I.B. Turkyilmaz, R. Yanardag, Gastroprotective effect of vitamin U in D-galactosamine-induced hepatotoxicity, J. Biochem. Mol. Toxicol. 36 (2022) e23124, https://doi.org/10.1002/jbt.23124.

[28] G. Bayrak, I.B. Turkyilmaz, R. Yanardag, The protective effect of vitamin U on pentylenetetrazole-induced brain damage in rats, J. Biochem. Mol. Toxicol. 36 (2022) e23169, https://doi.org/10.1002/jbt.23169.

[29] V.P. Shichkin, Vitamin B5 and vitamin U review: justification of combined use for the treatment of mucosa-associated gastrointestinal pathologies, Front. Pharmacol. 16 (2025) 1587627, https://doi.org/10.3389/fphar.2025.1587627.

[30] C. Ling, S. Liu, K. Meng, Y. Wang, X. Zhang, J. Liu, X. Li, K. Liu, H. Deng, C. Li, Vitamin U alleviates AFB(1)-induced hepatotoxicity in pregnant and lactating mice by regulating the Nrf2/Hmox1 pathway, Res. Vet. Sci. 180 (2024) 105436, https://doi.org/10.1016/j.rvsc.2024.105436.

[31] N. Wang, C. Zhang, Recent advances in the Management of Diabetic Kidney Disease: slowing progression, Int. J. Mol. Sci. 25 (2024), https://doi.org/10.3390/ijms25063086.

[32] C.Y. Jung, T.H. Yoo, Pathophysiologic mechanisms and potential biomarkers in diabetic kidney disease, Diabetes Metab. J. 46 (2022) 181–197, https://doi.org/10.4093/dmj.2021.0329.

[33] S.K. Sinha, M.B. Carpio, S.B. Nicholas, Fiery connections: macrophage-mediated inflammation, the journey from obesity to type 2 diabetes mellitus and diabetic kidney disease, Biomedicines 12 (2024), https://doi.org/10.3390/biomedicines12102209.

[34] J. Fu, Z. Sun, X. Wang, T. Zhang, W. Yuan, F. Salem, S.M. Yu, W. Zhang, K. Lee, J. C. He, The single-cell landscape of kidney immune cells reveals transcriptional heterogeneity in early diabetic kidney disease, Kidney Int. 102 (2022) 1291–1304, https://doi.org/10.1016/j.kint.2022.08.026.

[35] X. Li, M. Chen, J. Cao, X. Chen, H. Song, S. Shi, B. He, B. Zhang, Z. Zhang, Human umbilical cord mesenchymal stem cell-derived exosomes mitigate diabetic nephropathy via enhancing M2 macrophages polarization, Heliyon 10 (2024) e37002, https://doi.org/10.1016/j.heliyon.2024.e37002.

[36] C. Yuanchun, J. Jiaxing, L.I. Qingmin, Z. Xiaohong, J. Xiaofei, G. Weijuan, C. Xiangmei, Y.U. Wentao, Exploring the mechanism of Shenhua tablet alleviating renal injury by regulating macrophage glycolysis hypoxia-inducible factor-1α/pyruvate kinase M2 signaling pathway in diabetic kidney disease mice, J Tradit Chin Med 45 (2025) 528–537, https://doi.org/10.19852/j.cnki.jtcm.2025.03.009.

[37] X. Feng, W. Chen, X. Ni, P.J. Little, S. Xu, L. Tang, J. Weng, Metformin, Macrophage Dysfunction and Atherosclerosis, Front Immunol 12 (2021) 682853, https://doi.org/10.3389/fimmu.2021.682853.

[38] B. Rong, H. Jiang, W. Zhu, G. Yang, X. Zhou, Z. Lyu, X. Li, J. Zhang, Unraveling the role of macrophages in diabetes: impaired phagocytic function and therapeutic prospects, Medicine (Baltimore) 104 (2025) e41613, https://doi.org/10.1097/md.0000000000041613.

[39] X. Han, J. Zhang, L. Zhou, J. Wei, Y. Tu, Q. Shi, Y. Zhang, J. Ren, Y. Wang, H. Ying, G. Liang, Sclareol ameliorates hyperglycemia-induced renal injury through inhibiting the MAPK/NF-κB signaling pathway, Phytother. Res. 36 (2022) 2511–2523, https://doi.org/10.1002/ptr.7465.

[40] S.C.W. Tang, W.H. Yiu, Innate immunity in diabetic kidney disease, Nat. Rev. Nephrol. 16 (2020) 206–222, https://doi.org/10.1038/s41581-019-0234-4.

[41] K. Wu, H. Zha, T. Wu, H. Liu, R. Peng, Z. Lin, D. Lv, X. Liao, Y. Sun, Z. Zhang, Cytosolic Hmgb1 accumulation in mesangial cells aggravates diabetic kidney disease progression via NFκB signaling pathway, Cell. Mol. Life Sci. 81 (2024) 408, https://doi.org/10.1007/s00018-024-05433-7.

[42] Y.C. Yang, Y. Chien, A.A. Yarmishyn, L.Y. Lim, H.Y. Tsai, W.C. Kuo, P.H. Tsai, S. H. Yang, S.I. Hong, S.J. Chen, D.K. Hwang, Y.P. Yang, S.H. Chiou, Inhibition of oxidative stress-induced epithelial-mesenchymal transition in retinal pigment epithelial cells of age-related macular degeneration model by suppressing ERK activation, J. Adv. Res. 60 (2024) 141–157, https://doi.org/10.1016/j.jare.2023.06.004.

[43] S. Liu, S. Deng, Y. Ding, J.J. Flores, X. Zhang, X. Jia, X. Hu, J. Peng, G. Zuo, J. H. Zhang, Y. Gong, J. Tang, Secukinumab attenuates neuroinflammation and neurobehavior defect via PKCβ/ERK/NF-κB pathway in a rat model of GMH, Exp. Neurol. 360 (2023) 114276, https://doi.org/10.1016/j.expneurol.2022.114276.

[44] H.H. Liu, P. Lu, Y. Guo, E. Farrell, X. Zhang, M. Zheng, B. Bosano, Z. Zhang, J. Allard, G. Liao, S. Fu, J. Chen, K. Dolim, A. Kuroda, J. Usuka, J. Cheng, W. Tao, K. Welch, Y. Liu, J. Pease, S.A. de Keczer, M. Masjedizadeh, J.S. Hu, P. Weller, T. Garrow, G. Peltz, An integrative genomic analysis identifies Bhmt2 as a diet-

dependent genetic factor protecting against acetaminophen-induced liver toxicity, Genome Res. 20 (2010) 28–35, https://doi.org/10.1101/gr.097212.109.
[45] S.S. Szegedi, C.C. Castro, M. Koutmos, T.A. Garrow, Betaine-homocysteine S-methyltransferase-2 is an S-methylmethionine-homocysteine methyltransferase, J. Biol. Chem. 283 (2008) 8939–8945, https://doi.org/10.1074/jbc.M710449200.
[46] F. Mirzadeh Azad, E.A. Struys, V. Wingert, L. Hannibal, K. Mills, J.H. Jansen, D. B. Longley, H.G. Stunnenberg, Y. Atlasi, Spic regulates one-carbon metabolism and histone methylation in ground-state pluripotency, Sci. Adv. 9 (2023) eadg7997, https://doi.org/10.1126/sciadv.adg7997.
[47] Y.J. Suzuki, M.V. Lorenzi, S.S. Shi, R.M. Day, J.B. Blumberg, Homocysteine exerts cell type-specific inhibition of AP-1 transcription factor, Free Radic. Biol. Med. 28 (2000) 39–45, https://doi.org/10.1016/s0891-5849(99)00200-2.
[48] K. Robert, C. Pagès, A. Ledru, J. Delabar, J. Caboche, N. Janel, Regulation of extracellular signal-regulated kinase by homocysteine in hippocampus, Neuroscience 133 (2005) 925–935, https://doi.org/10.1016/j.neuroscience.2005.03.034.
[49] R.F. Zanin, L.S. Bergamin, F.B. Morrone, R. Coutinho-Silva, A.T. de Souza Wyse, A. M. Battastini, Pathological concentrations of homocysteine increases IL-1β production in macrophages in a P2X7, NF-κB, and erk-dependent manner, Purinergic Signal 11 (2015) 463–470, https://doi.org/10.1007/s11302-015-9464-5.
[50] S.N. Deep, S. Seelig, S. Paul, R. Poddar, Homocysteine-induced sustained GluN2A NMDA receptor stimulation leads to mitochondrial ROS generation and neurotoxicity, J. Biol. Chem. 300 (2024) 107253, https://doi.org/10.1016/j.jbc.2024.107253.

Supplementary material

S-methylmethionine Ameliorates Renal Injury in Diabetic Mice by Modulating Macrophage Inflammaging via ERK/NF-κb Signaling Pathway

Hao Dong, Linjie Shen, Pawuziya Abulizi, Yuezhang Sun, Lulingxiao Nie, Aimin Cui, Qian Fu, Ning Ji, Yuwen Luo, Chienshan Chen, Aimin Xu, Wai Keung Leung*, Qi Wang*

Table S1. Primer sequence of target genes used for qPCR.

Gene Name	Species	Forward 5'-3'	Reverse 5'-3'
Nos2	Mouse	GGTGAAGGGACTGAGCTGTT	ACGTTCTCCGTTCTCTTGCAG
Arg1	Mouse	GTACATTGGCTTGCGAGACG	ATCGGCCTTTTCTTCCTTCCC
Fos	Mouse	CGGGCTTTCCCCAAACTTCG	GTGTTGACAGGAGAGCCCAT
Jun	Mouse	GGGAGCATTTGGAGAGTCCC	TTTGCAAAAGTTCGCTCCCG
Mmp9	Mouse	AAACCTCCAACCTCACGGAC	TTGGAATCGACCCACGTCTG
Ptgs2	Mouse	TCCATTGACCAGAGCAGAGA	TCTGGACGAGGTTTTTCCAC
Actb	Mouse	AAATCGTGCGTGACATCAAAA	TCTCCAGGGAGGAAGAGGAT

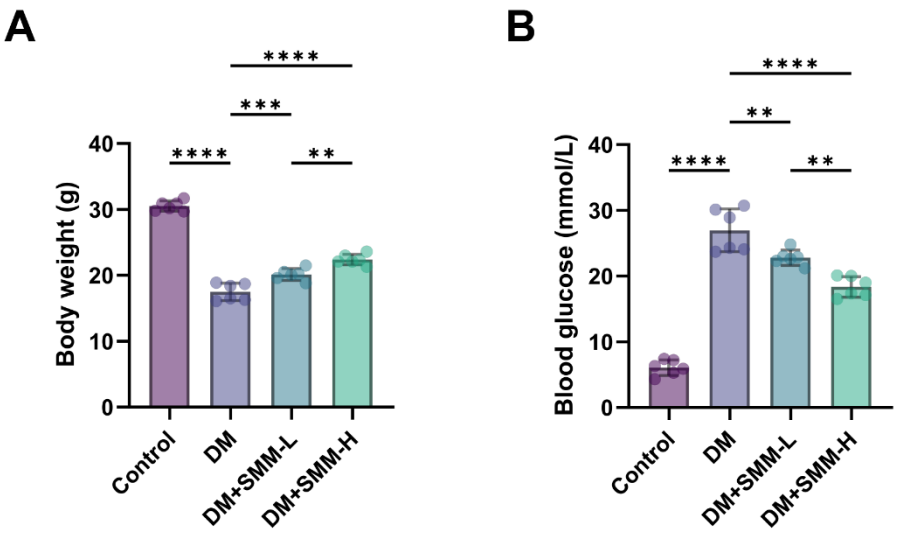

Fig. S1. Body weight and blood glucose levels of mice at week 10.

Analyses of (A) Body weight, and (B) Blood glucose of each group at week 10. Data are presented as mean ± SD (n = 6). *p < 0.05, **p < 0.01, ***p < 0.001, ****p < 0.0001.

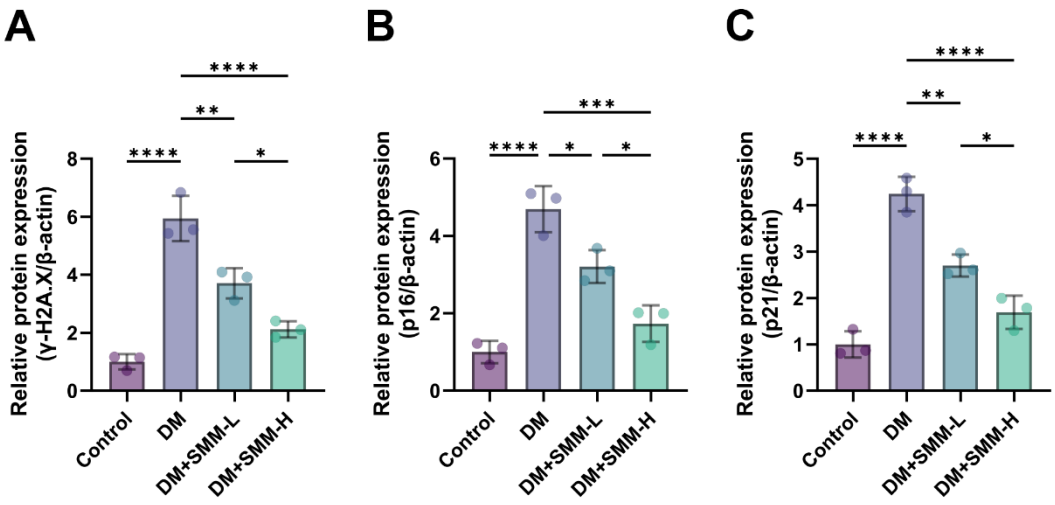

Fig. S2. Quantitative analysis of Western blot bands for senescence-related proteins in kidney tissues.

Relative protein levels of (A) γ-H2A.X, (B) p16, and (C) p21. Data are presented as mean ± SD (n = 3). *p < 0.05, **p < 0.01, ***p < 0.001, ****p < 0.0001.

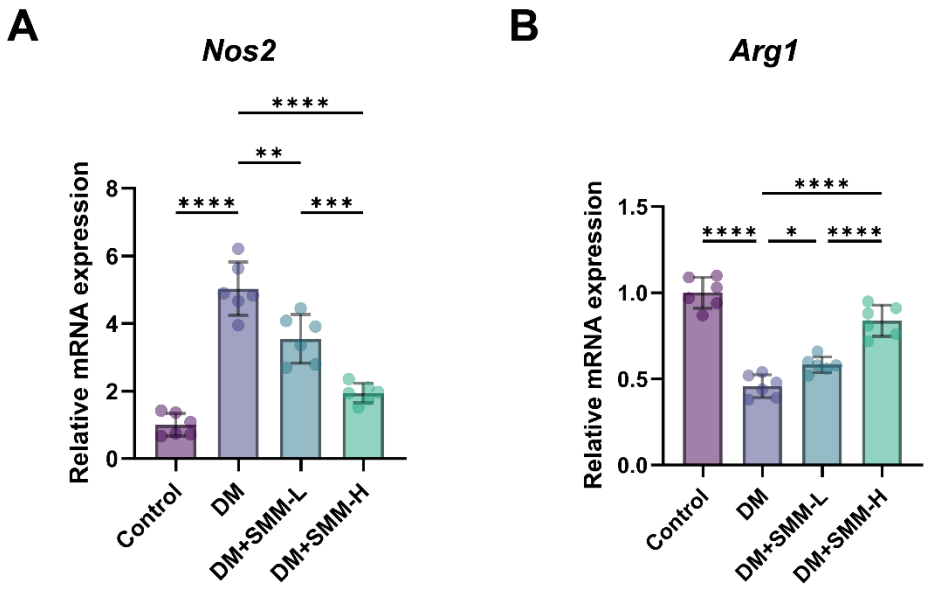

Fig. S3. Quantitative analysis of Macrophage Polarization-Related Marker Genes by RT-qPCR.

Relative mRNA levels of (A) nitric oxide synthase 2 (*Nos2*), and (B) arginase-1 (*Arg1*). Data are presented as mean ± SD (n = 6). *p < 0.05, **p < 0.01, ***p < 0.001, ****p < 0.0001.

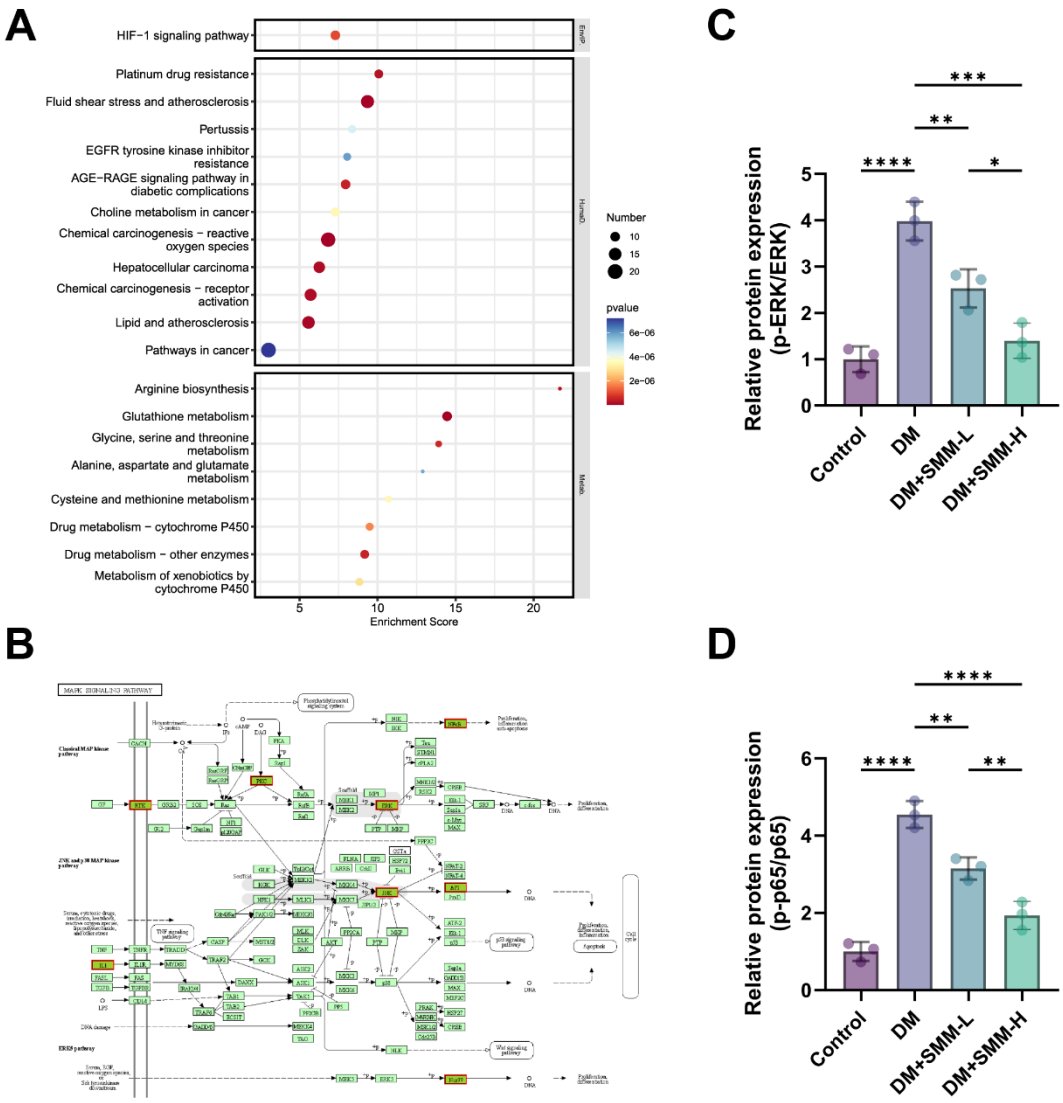

Fig. S4. KEGG pathway enrichment analysis and MAPK signaling pathway.

(A) KEGG pathway enrichment analysis of common targets. (B)Visualization of potential targets of SMM acting on the MAPK signaling pathway. Relative protein levels of (C) p-ERK/ERK, and (D) p-p65/p65. Data are presented as mean ± SD (n = 3). *p < 0.05, **p < 0.01, ***p < 0.001, ****p < 0.0001.

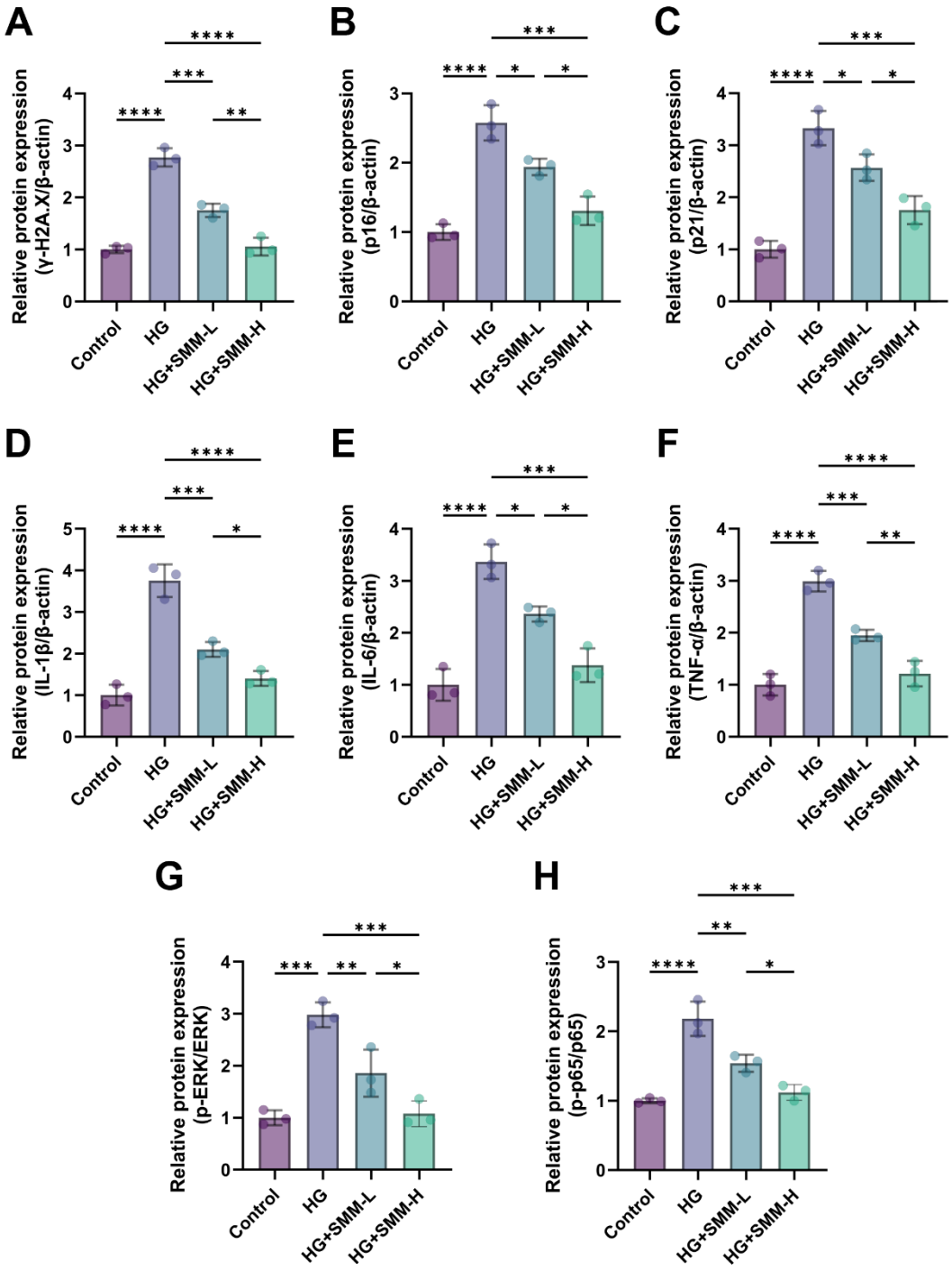

Fig. S5. Quantitative analysis of Western blot bands in RAW264.7 cells.

Relative protein levels of (A) γ-H2A.X, (B) p16, (C) p21, (D) IL-1β, (E) IL-6, (F) TNF-α, (G) p-ERK/ERK, and (H) p-p65/p65. Data are presented as mean ± SD (n = 3). *p < 0.05, **p < 0.01, ***p < 0.001, ****p < 0.0001.

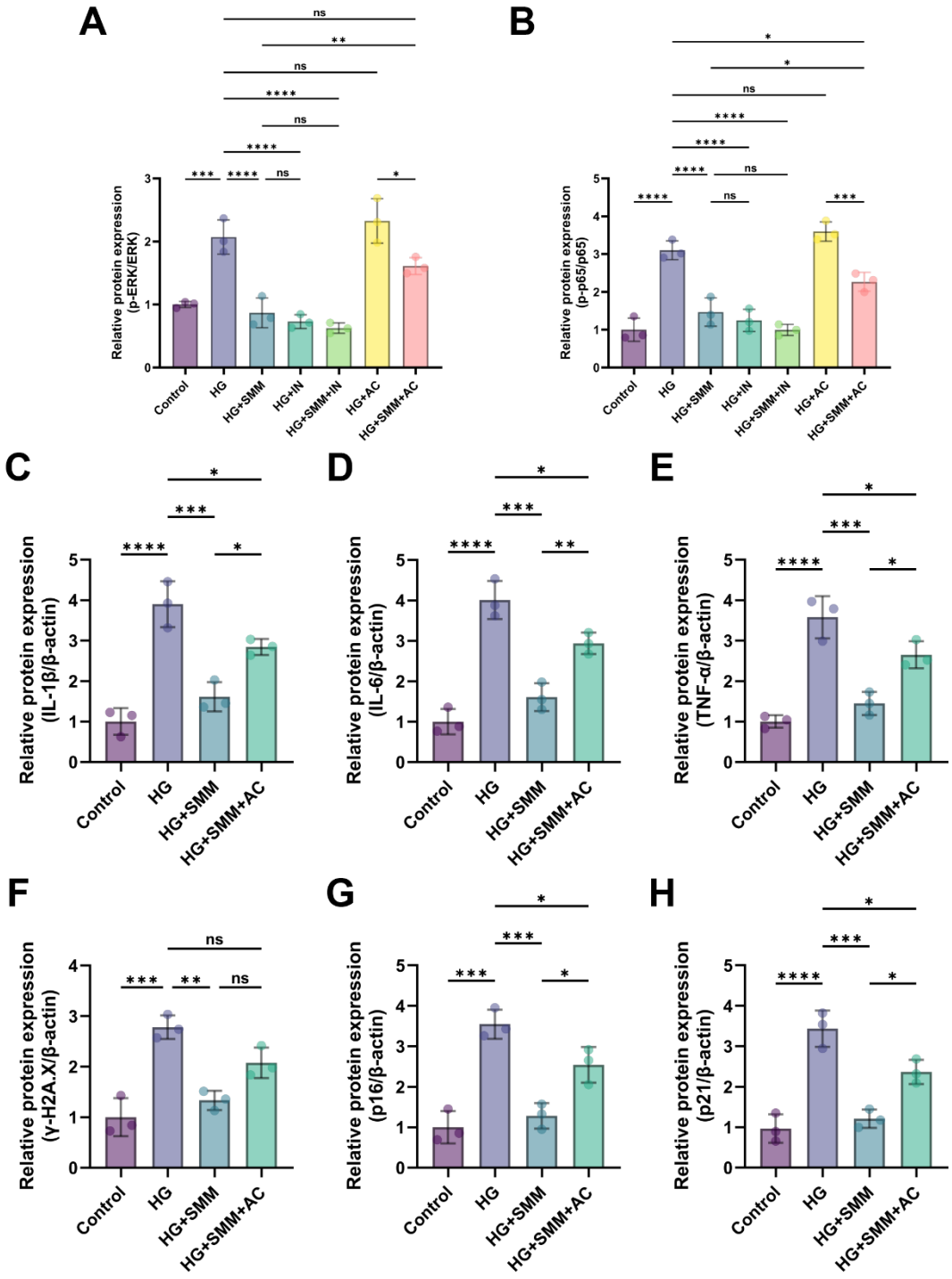

Fig. S6. Quantitative analysis of Western blot bands in RAW264.7 cells using ERK inhibitor or activator.

Relative protein levels of (A) p-ERK/ERK, (B) p-p65/p65, (C) IL-1β, (D) IL-6, (E) TNF-α, (F) γ-H2A.X, (G) p16, and (H) p21. Data are presented as mean ± SD (n = 3). *p < 0.05, **p < 0.01, ***p < 0.001, ****p < 0.0001.

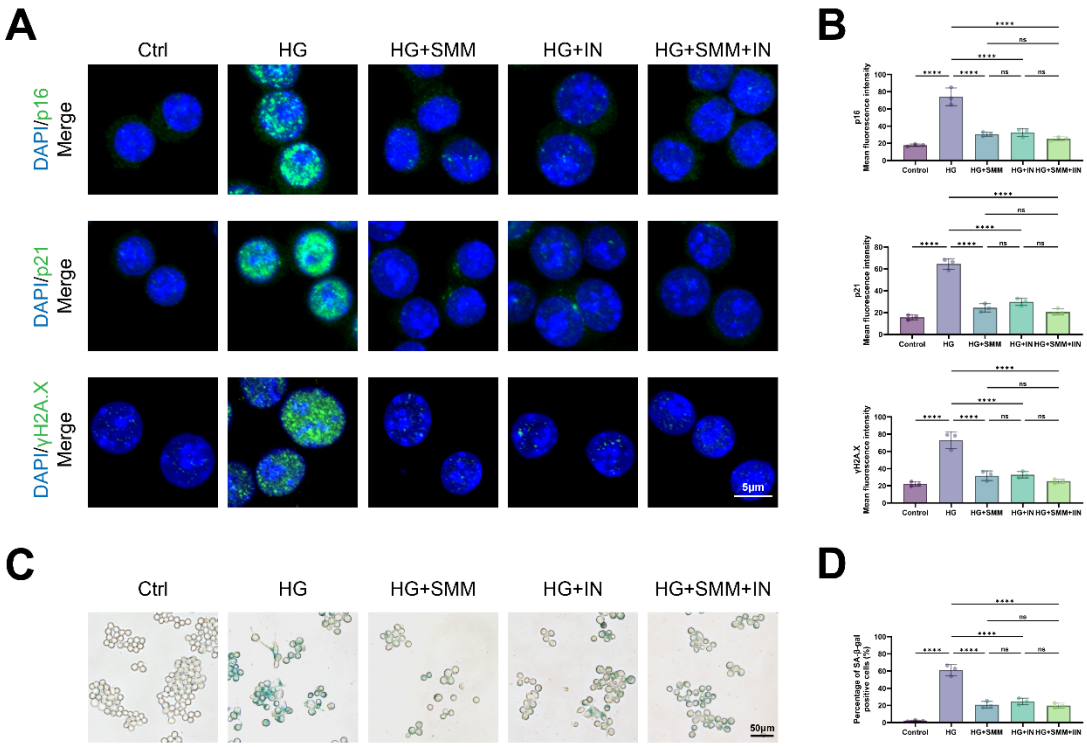

Fig. S7. Inhibiting the ERK/NF-κB signaling pathway reduces macrophage aging.

(A-B) Representative immunofluorescence staining and quantitative analysis of p16, p21, and γ-H2A.X in RAW264.7 cells. (C-D) Cellular senescence assessed by SA-β-gal staining and quantitative analysis. Data are presented as mean ± SD (n = 3). *p < 0.05, **p < 0.01, ***p < 0.001, ****p < 0.0001.